remote sensing

MDPI

Article

Long-Term Variability in Sea Surface Temperature and Chlorophyll *a* Concentration in the Gulf of California

Juana López Martínez [1], Edgardo Basilio Farach Espinoza [1], Hugo Herrera Cervantes [2,*] and Ricardo García Morales [3]

[1] Centro de Investigaciones Biológicas del Noroeste S.C. Unidad Sonora, Km. 2.35 Camino al Tular, Estero de Bacochibampo, Guaymas 85465, Sonora, Mexico; jlopez04@cibnor.mx (J.L.M.); efarach@pg.cibnor.mx (E.B.F.E.)
[2] Centro de Investigación Científica y de Educación Superior de Ensenada, Unidad La Paz, Calle Miraflores No. 334 e/Mulegé y La Paz, La Paz 23050, Baja California Sur, Mexico
[3] CONACYT, Unidad Nayarit del Centro de Investigaciones Biológicas del Noroeste S.C. (UNCIBNOR), Calle Dos No. 23, Cd. del Conocimiento, Cd. Industrial, Av. Emilio M. González, Sin Referencia, Tepic 63173, Nayarit, Mexico; rgarcia@cibnor.mx
* Correspondence: hherrera@cicese.mx

Abstract: The Gulf of California (GC) is the only interior sea in the Eastern Pacific Ocean and is the most important fishing area in the northwestern region of the Mexican Pacific. This study focuses on the oceanographic variability of the GC, including its southern portion, which is an area with a high flow of energy and exchange of properties with the Pacific Ocean (PO), in order to determine its role in physical–biological cycles and climate change. The purpose of this work is to analyze the sea surface temperature (SST) and chlorophyll *a* concentration (Chl-a) during the period from 1998–2022 as indicators of long-term physical and biological processes, oceanographic variability, and primary production in the GC. In total, 513 subareas in the GC were analyzed, and a cluster analysis was applied to identify similar areas in terms of SST and Chl-a via the K-means method and using the silhouette coefficient (>0.5) as a metric to validate the clusters obtained. The trends of the time series of both variables were analyzed, and a fast Fourier analysis was performed to evaluate cycles in the series. A descriptive analysis of the SST and Chl-a series showed that the SST decreased from south to north. Six bioregions were identified using a combined of both SST and Chl-a data. The spectral analysis of the SST showed that the main frequencies in the six bioregions were annual and interannual (3–7 years), and the frequencies of their variations were associated with basin-level weather events, such as El Niño and La Niña. The SST in the GC showed a heating trend at an annual rate of ~0.036 °C (~0.73 °C in 20 years) and a decrease in Chl-a at an annual rate of ~0.012 mg/m^3 (~0.25 mg/m^3 in 20 years), with potential consequences for communities and ecosystems. Additionally, cycles of 10–13 and 15–20 years were identified, and the 10–13-year cycle explained almost 40–50% of the signal power in some regions. Moreover, mesoscale features (eddies and filaments) were identified along the GC, and they were mainly associated with the clusters of the SST. All these spatial and temporal variabilities induce conditions that generate different habitats and could explain the high biodiversity of the GC. If the warming trend of the SST and the decreasing trend of the Chl-a continue in the long term, concerns could be raised, as they can have important effects on the dynamics of this important marine ecosystem, including habitat loss for numerous native species, declines in the catches of the main fishery resources, and, consequently, support for the arrival of harmful invasive species.

Keywords: environmental variability; oceanographic dynamics; mesoscale phenomena; Gulf of California; SST, Chl-a, ENSO, and PDO

Citation: López Martínez, J.; Farach Espinoza, E.B.; Herrera Cervantes, H.; García Morales, R. Long-Term Variability in Sea Surface Temperature and Chlorophyll *a* Concentration in the Gulf of California. *Remote Sens.* **2023**, *15*, 4088. https://doi.org/10.3390/rs15164088

Academic Editors: José C.B. da Silva, Jorge M. Magalhaes and Caixia Wang

Received: 19 June 2023
Revised: 13 August 2023
Accepted: 14 August 2023
Published: 19 August 2023

1. Introduction

The GC is a marginal sea surrounded by the semi-desert of northern Mexico, which divides the Baja California Peninsula (BCP) from the Mexican mainland and is approximately 1200 km long and 80–200 km wide [1–3]. On the surface, the GC shows the presence of different water masses, including California current water, tropical surface water, and the GC water, which originates in the northern Gulf and is found in the upper layer (<200 m), with temperature and salinity typical of the GC [4]. The GC (Figure 1) is the most important fishing region in the northwestern area of the Mexican Pacific. It is one of the marine systems that is most closely observed by the worldwide conservation sector, and there is a scientific research focus on the detection of the impacts of anthropogenic climate change on coastal ecosystems, including on some small pelagic fish, shrimps, and jellyfish [2,5–9]. Variations in these ecosystems have been attributed to large fishing efforts, overfishing, and environmental factors, which can alter natural mortality in early life stages and have effects on new-generation recruitment in the adult fish population [10] in addition to the potential entry of invasive species.

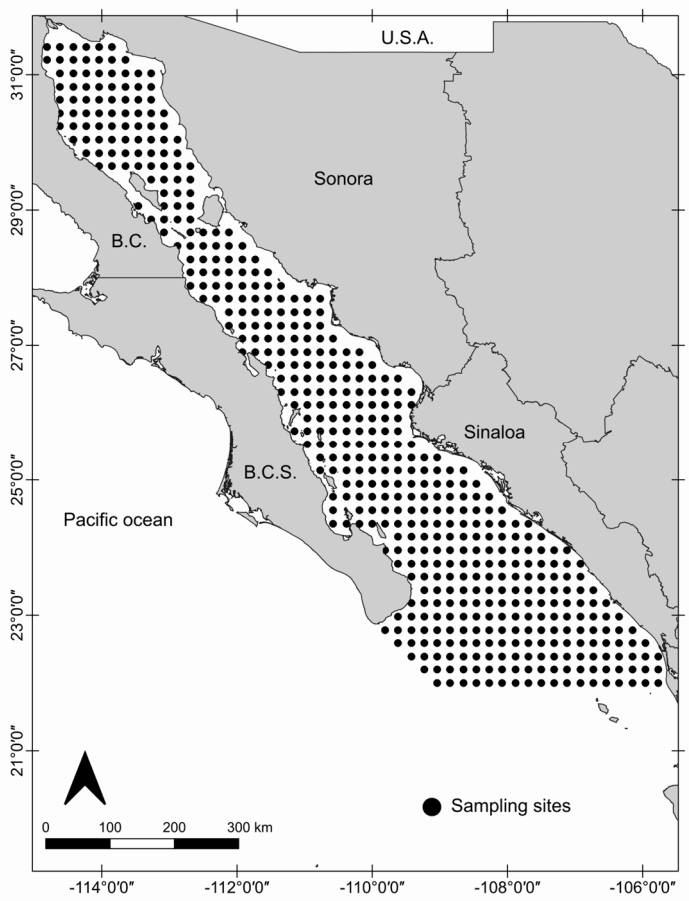

Figure 1. Study area and localization of the sampling sites for the analyses of the SST and Chl-a in the GC during the period from 1998–2022.

Circulation studies have indicated that the combined action of wind forcing, the PO's influence at the gulf's mouth, tides, and solar radiation creates a typical circulation pattern, resulting in anticyclonic circulation during the winter and cyclonic circulation during the summer [11,12], which suggests that inflow occurs next to the southern coast of the mainland and that outflow occurs next to the tip of the coast of the BCP. This mainly causes changes on the annual and semiannual temporal scales, so it is important to delimit the fronts and gradients of SST in semi-closed areas such as the GC. This circulation includes mesoscale structures such as filaments, meanders, and eddies, which transfer

important properties from one coast to another [13], influence the mixed-layer depth [12], and exhibit different spatiotemporal scales [14,15]. Mesoscale eddies can be identified by their gradients of temperature and photosynthetic pigments; their dynamic properties allow them to transfer heat, salt, and nutrients to the water column [16]. They can be generated by different pressure phenomena, by ocean–atmosphere interchange, and by mixing of different masses of water, currents, and irregularities in the coastline, islands, or capes [17,18]. Cyclonic eddies present a counterclockwise rotation and have cold cores and one outcrop thermocline, while anticyclonic eddies present a clockwise rotation and possess warmer cores [19,20]; nevertheless, during warm conditions, anticyclonic eddies can display higher productivity than cyclonic ones due to a weaker stratification [21]. In many cases, the anticyclonic eddies concentrate pigments, causing an increase in Chl-a in its center [22,23]. The use of satellite images allows a synoptic analysis of the distribution and spatiotemporal variability of mesoscale phenomena such as eddies, upwelling, and filaments in areas influenced by marine current systems [24,25], contributing to the continuous observation of the environmental variability in large marine ecosystems.

Ripa [26,27] and Beier and Ripa [28] suggested that annually, the PO forces an internal baroclinic Kelvin wave that enters the gulf on the continental coast, causing a cyclonic circulation coastline. This explains the seasonal pattern of circulation and the interchanges of temperature and salinity observed in the GC [29–31]. Through hydrographic studies, it has been found that in winter, the oceanic forcing is associated with the influx of cold water with high salinity for the tip of the coast of the BCP, whereas in summer, there is a water intrusion along the mainland coast of the GC [12,32,33]. This inflow and outflow of water along the coast and the interaction with the coast generate cyclonic and anticyclonic mesoscale gyres. Recently, studies have shown a relationship of the increase or decrease in SST and Chl-a concentration values with the presence of mesoscale phenomena in the GC [34–36].

The wind patterns and the air–sea heat exchanges observed in the GC during the annual cycle are characterized by northwesterly strong winds from November to May and weak southwesterly winds with frequent calms in summer [37,38]. Under winter conditions, the gulf shows upwelling processes and high primary productivity levels on the mainland coast, caused by strong northwest winds that induce Ekman transport, which generates the coastal upwelling, increasing the phytoplankton biomass. However, under summer conditions (weak southwesterly winds), the water column is strongly stratified, weakening the upwelling processes [39]. These high productivity levels make the GC an important fishing zone, with enterprises ranging from highly industrialized pelagic fisheries to coastal artisanal fisheries, which obtain different products with high economic value in terms of economic income, employment, and social impact, such as large pelagic fish (tuna and marlin), small pelagic fish (sardine and anchovy), shrimp, as well as squid; the associated catch volumes largely depend on the availability of food in the first trophic levels [39].

The interannual variability of the ecological and oceanographic features in the GC is significantly influenced by the PO. The presence of the El Niño (ENSO) events (the main frequency of variation in interannual scales) [40] is associated with changes in the ocean–atmosphere forcing and northward propagation of warm waters along the mainland coast [41]. Strub and James [42] suggested that the link of the ENSO signals to the NE Pacific is given by two physical mechanisms: (1) through by an increase in poleward winds caused by changes in the equatorial zone atmospheric circulation [43] and (2) the poleward advection of water along the coast and characterized by changes in water temperature, sea-level rises, climatic meteorological variations, and poor biological productivity. Filonov and Tereschenko [44] used hydrographic observations along the west coast of Mexico during the strong El Niño of 1997–1998 to analyze the poleward propagation of this phenomena, suggesting that water masses of the equatorial that occupied the surface were carried by these coastal-trapped waves, deepened the thermocline, and replaced local water in the surface.

The presence of the ENSO signals within the GC and Its relationship with the physical and biological processes have been documented in several studies [34,39,41,42,45]. Lavín et al. [46] found a significant relationship between the Southern Oscillation Index (SOI) and a spatially averaged anomaly time series of the GC, mainly during the strongest ENSO events. Likewise, Sánchez-Cabeza et al. [47] found a significant positive correlation between the Oceanic El Niño Index (ONI) and SST anomalies. During La Niña events, negative anomalies (up to 4 °C) were identified, and during El Niño events, positive anomalies (up to 7 °C) in the minimum SST in the southern GC region were documented [47]. The minimal positive SST anomalies were caused by (i) inhibition of the coastal upwelling and (ii) limited cold-water intrusion from the California current, and the rapid warming rate could be due to (i) the shallowness and coastal dynamics, (ii) warmer surface tropical waters the Mexican coastal current, (iii) the transport of warmer waters from the western Pacific during El Niño, and (iv) global warming.

Herrera-Cervantes et al. [48] studied the relationship between the spatial signatures of ENSO and satellite-derived Chl-a trends showing the coherence between the spatial distribution of the EOF amplitudes and the MEI correlation coefficients. Lluch-Belda et al. [49] proved that, when considering SST in the GC since the early 1960s, no significant trends could be detected, and in fact, the slope was negative. Robles-Tamayo et al. [40] used a spectral analysis to show that the interannual frequencies of the SST in the GC southern region were associated with the climatological phenomena of El Niño y La Niña, and Lluch-Cota et al. [41] found coherent trends among SST series, ecological components of the GC, and the Pacific decadal oscillation (PDO).

Several regionalizations of the GC have been proposed [50–52], as the natural regions are areas that share the same environment and, in many cases, biological characteristics. Regionalization can be conducted by using direct or indirect methods, thus enabling the study of large areas through patterns of similar variations. For this, different indicators are used (SST, water masses, physical barriers, types of climate, bathymetry, and productive zones) to regionalize an area through the grouping of specific features [53]. To perform regionalization based on indirect methods, SST and satellite images of Chl-a concentration have been used, highlighting that the regionalization of an area helps to manage the biological resources of that system [54]. Based on oceanographic information obtained through remote sensing and historical in situ data, Petatán-Ramírez [51] proposed an oceanographic zonation of the GC with 14 oceanographic regions, while Heras-Sánchez et al. [52] proposed the separation of the GC into 12 regions, in which the eutrophic zones (coastal) covered 15% of the area and contributed to 38% of the total Chl-a estimated.

In this work, we explored the monthly, seasonal, and interannual variability of the SST and Chl-a at 513 stations in the GC for the period from 1998–2022 and included a regionalization based on a cluster analysis with the purpose of grouping the sampling points with the greatest homogeneity in SST and Chl-a concentration, which were obtained through monthly composite satellite images.

2. Materials and Methods

2.1. Study Area

The GC exhibits complex climatic, oceanographic, and ecological characteristics due to its location in the temperate–tropical transition zone [42,55]. The PO, wind forcing, and heat interchanges determine the general circulation in the GC [56]. The southern region is a transitional zone where different masses of water meet, thus displaying a complex thermohaline circulation generating mesoscale phenomena that are visible in satellite images [57].

2.2. Environmental and Oceanographic Characterization

For environmental and oceanographic analyses, a composite of satellite images of SST (°C) and Chl-a (mg/m^3) with a spatial resolution of one km were used; they were supplied by Mati Kahru (Scripps Institution of Oceanography). Composites of the satellite

images from the MODIS-Aqua, Terra, and VIIRS sensors were used for the SST analysis during the period from 2000–2022; for the period from 1998–1999, monthly SST satellite images from the AVHRR sensor (available at https://www.ncei.noaa.gov/products/avhrr-pathfinder-sst (accessed on 21 February 2023)) were processed. Additionally, a composite of monthly images from the MODIS-Aqua, Terra, VIIRS, SeaWiFS, and OLCI sensors were used for the analysis of the Chl-a. The monthly images of the SST and Chl-a are available at http://spg-satdata.ucsd.edu (accessed on 23 January 2023). The images were in HDF (hierarchical data format), and the SST and Chl-a values used 1 byte per pixel, with linear scaling for SST (°C = 0.15 × PV − 3.0) and logarithmic scaling for Chl-a ($mg/m^3 = 10(0.015 * PV - 2.0)$). Image processing and analysis were performed with the Windows Image Manager (WIM/WAM) [58].

To obtain the values of SST and Chl-a, 513 subareas were selected in the GC (Figure 1). Each subarea represented an area of 400 km^2 (20 × 20 km). Mean SST and Chl-a values were obtained from ~400 pixels in each subarea, with a total of 300 SST images and 300 Chl-a images for the 25 years of study. The analysis covered a total of 205,000 km^2, which represents 82% of the total marine surface of the GC's approximate 247,000 km^2 [59].

We carried out the cluster analysis using both variables (SST and Chl-a) together. We used fuzzy clustering methods as the grouping method. The partitional clustering method K-means of Ralambondrainy [60], Koren et al. [61], and Li et al. [62] is the division of data objects into non-overlapping subsets such that each data object is in exactly one subset. The K-means algorithm proposed by MacQueen [63] is an algorithm that allows discovering clusters in datasets; each cluster is associated with a centroid (center point), and each data object is assigned to the cluster with the closest centroid. The method by which K-means algorithm works is as follows:

1. Initialize centroids by first shuffling the dataset and then randomly selecting K data points for the centroids without replacement;
2. Keep iterating until there is no change to the centroids; i.e., the assignment of data points to clusters does not change;
3. Compute the sum of the squared distance between data points and all centroids;
4. Assign each data point to the closest cluster (centroid);
5. Compute the centroids for the clusters by taking the average of the all data points that belong to each cluster.

Once the groups were attained for both environmental variables, a contingency analysis was applied to validate ($p < 0.05$) the dissimilarities from the clusters obtained.

The relationship between SST and Chl-a was evaluated by means of nonlinear estimation. Subsequently, the SST and Chl-a climatology from each cluster was estimated, and the anomalies were built based on the time series of each one of the clusters; the seasonal cycle was removed by subtracting the monthly average climatology on a cluster-by-cluster basis. The interannual variability was evaluated with a time-series analysis (fast Fourier transform) of each one of the clusters obtained from the cluster analysis, and cross-correlation analysis was executed between the SST and the El Niño ONI and PDO index. The ONI was used as a quantitative measure of the remote forcing associated with the intensity of equatorial Pacific ENSO events. The PDO index is often described as a long-lived El-Niño-like pattern of Pacific climate variability [64]. All of the analyses were performed in Statistical Software version 7.5 and PAST version 4.12.

Based on the study of Farach-Espinoza et al. [35] that determined the annual and interannual frequency and duration of mesoscale processes (eddies, coastal upwelling, cold filaments, and water mass intrusion) in the GC during the period from 1998–2018, by analyzing a composite of 1 km resolution, 5-day SST and Chl-a satellite images, in this study, random years were chosen for their satellite images to be processed and for the presence of mesoscale features to be identified by using criteria from previous studies in which visual inspection was used to identify mesoscale features by following thermal and primary production fronts [34,65]. Additionally, the method of Kahru et al. [19] was followed, in which the front detection method of Cayula and Cornillon [66] was applied

via the subroutine Single-Image Edge Detection (SIED) in WIMSoft® (San Diego, CA, USA). Finally, we applied a modification proposed by Diehl et al. [67] to detect the edges in the one-month satellite images of both Chl-a and SST. The identified eddies were validated by assessing images of sea water velocity available at https://resources.marine.copernicus.eu (accessed on 29 January 2023).

3. Results

3.1. Cluster Analysis

The values of the silhouette coefficient need to be greater than 0.5 to significantly discriminate the groups from each other; therefore, six clusters were identified from the K-mean cluster analysis of SST and Chl-a (Figure 2). This result allowed analysis of the time series, climatology, and interannual variability of each cluster individually. Through this cluster analysis, six bioregions were obtained in the study area, which are spatially distributed in Figure 3.

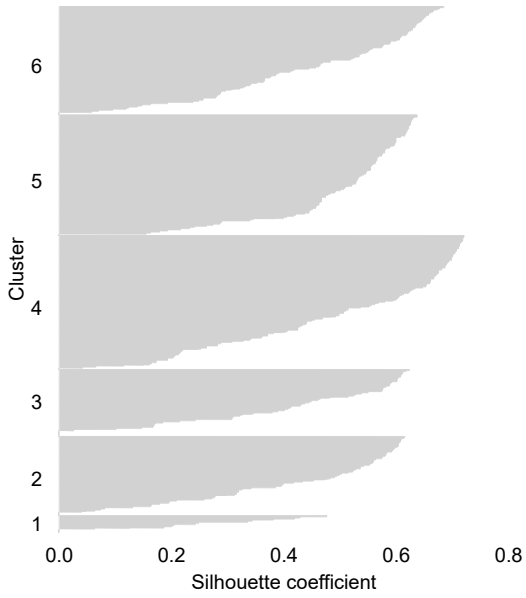

Figure 2. Silhouette coefficient from the K-means cluster analysis of SST and Chl-a concentration in the subareas of the GC.

Through the contingency analysis, it was estimated that there were no associations ($p < 0.05$) between clusters identified for SST and for Chl-a (Table 1), thus validating further analyses of the six clusters individually.

Table 1. Contingency analysis of the clusters obtained in the GC.

	Pearson's Chi-Square Test				
	N	**Chi-Square**	**Chi-Square (Critical)**	**d.f.**	***p*-Value**
SST	72	2.784	67.505	55	1
Chl-a	72	3.099		55	1

Figure 3 shows the spatial pattern of the six clusters, where most of the subareas were grouped according to their latitude except cluster 1, which is located along the mainland coast. Cluster 5 included the northernmost regions, areas with strong tidal and vertical mixing in the presence of seasonal heating and cooling [68] from the upper gulf to south of the Midriff Islands with an average depth of 200 m and characterized by connecting active basins to the west (Delfin, Wagner, Cerro Prieto, and Salton) and inactive basins to the east

(Tiburón and Aldair-Tepoca). These are wide and shallow with sediment packages of up to 6 km, a product of terrigenous input from the Colorado River, including the Midriff Islands, characterized by high vertical mixing, the main mechanism by which deeper-reaching nutrients ascend to the surface, creating the conditions for the high primary productivity observed in the upper GC–south of Midriff Islands area [69] (Table 2). In the Midriff Islands, there is a strong exchange between the north and the south [70,71]. Cluster 3 included the deep region (2000 m of depth) of the central gulf between 26° to 28°N, and it is characterized by large water courses and a narrow and elongated basin, with sedimentary thickness of up to 1 km, connected by a well-defined arrangement of faults, which develop over oceanic crust (Guaymas and part of the Carmen Basin), and where jets and mesoscale gyres are located roughly over Carmen Basin [71]. This region is encompassed by areas that are under the influence of summer and winter coastal upwelling [12]. Cluster 6 comprised the limit between Sonora and Sinaloa (24° to 26°N), including Farallon, Carmen, and Pescadero Basins, with depths between 500 to 2000 m. In this area, the basins are characterized by deep waters and low sedimentation rates and are strongly fractured by subsidiary structures (Table 2), where the surface circulation appears to be dominated by mesoscale eddies structures that have an alternating sense of rotation [71]. Cluster 4 included the oceanic region of the southern GC surrounding areas down to the southern tip of Baja California Peninsula, including Pescadero and Alarcon Basins, where the anticyclonic gyres observed during summer may be caused by instabilities of the poleward propagation of coastally trapped waves along the mainland coast of GC [71]. While cluster 2 comprised the area around the entrance of the gulf, including the southern coastal region of Sinaloa (mainland coast), cluster 1 included only the coastal area of Sinaloa in which important upwelling events occur during winter and spring, and together with discharges from rivers and coastal lagoons, these contribute to the high primary productivity observed in this region (Table 2).

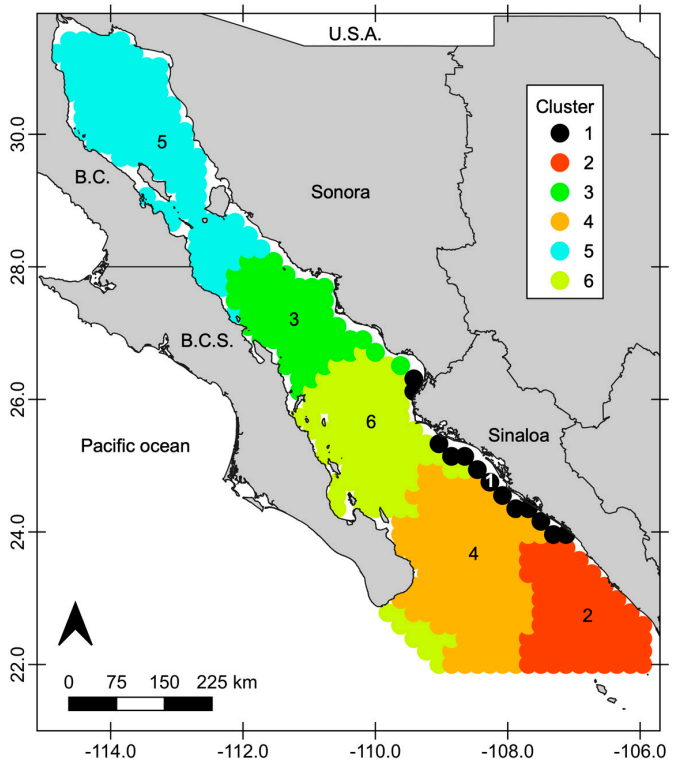

Figure 3. Bioregions in the Gulf of California obtained from the clustering of SST and Chl-a concentration.

Table 2. The bioregions derived from the combination of the clusters for SST and Chl-a in the GC.

Region	Cluster	Sea Surface Water Characteristics
Upper GC–south of Midriff Islands	5	Cold water (23.43 °C), eutrophic (1.81 mg/m^3)
Central gulf between 26° to 28°N	3	Intermediate water (24.59 °C), eutrophic (1.53 mg/m^3)
Limit between Sonora and Sinaloa (24° to 26°N)	6	Intermediate water (25.46 °C), mesotrophic (0.92 mg/m^3)
Northern and central coast of Sinaloa	1	Warm water (25.99 °C), eutrophic (1.49 mg/m^3)
Oceanic region at the southern GC surrounding areas down to the southern tip of Baja California Peninsula	4	Warm water (26.29 °C), oligotrophic (0.37 mg/m^3)
Around the entrance of the gulf, including the southern coastal region of Sinaloa	2	Warm water (26.83 °C), mesotrophic (0.95 mg/m^3)

The mean values of the six bioregions were obtained, each one with a unique combination of temperature and Chl-a concentration values. For SST, the ranges were cold water (<24.5 °C), intermediate water (24.6–25.9 °C), and warm water (>25.9 °C); for Chl-a concentration, the ranges were oligotrophic water (0.1–0.5 mg/m^3), mesotrophic water (0.6–1 mg/m^3), and eutrophic water (>1.0 mg/m^3) (Table 2).

3.2. Time Series and Climatology

The time series of each cluster showed values of SST between 15 and 32 °C (Figure 4). Cluster 4 presented the highest values (between 19 and 32 °C (Table 3)), and cluster 5 presented the lowest (15 to 31 °C). On the other hand, the average Chl-a concentration was between 0.37 and 1.81 mg/m^3, with the lowest value in cluster 4 with 0.11 mg/m^3 and the highest values exhibited in cluster 1 with 11.13 mg/m^3 (Table 3).

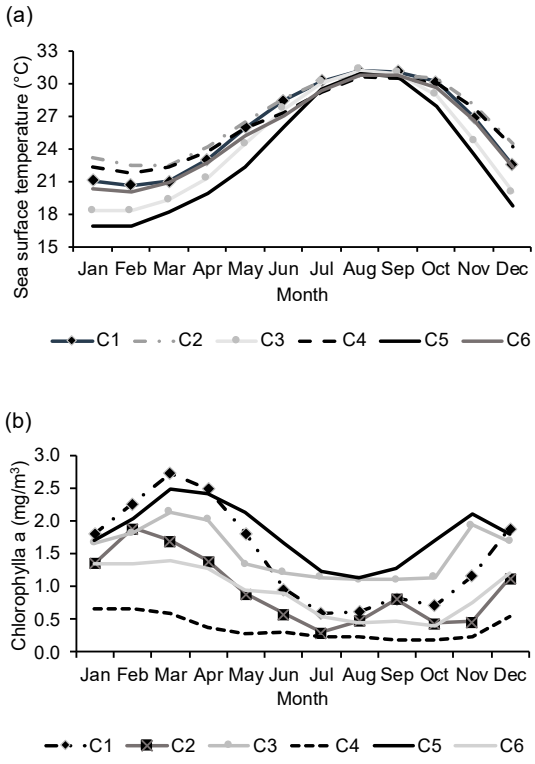

Figure 4. Climatology of the SST (**a**) and Chl-a concentration (**b**) of each cluster in the GC during the period from 1998–2022.

Table 3. SST and Chl-a concentration of each cluster in the GC.

Cluster	SST			Chl-a		
	Mean ± S.D. (°C)	Minimum (°C)	Maximum (°C)	Mean ± S.D. (mg/m^3)	Minimum (mg/m^3)	Maximum (mg/m^3)
1	25.99 ± 4.17	16.98	31.96	1.49 ± 1.27	0.28	11.13
2	26.83 ± 3.40	18.58	31.98	0.95 ± 1.02	0.13	8.89
3	24.59 ± 4.94	16.17	32.43	1.53 ± 0.49	0.84	3.08
4	26.29 ± 3.32	19.62	31.66	0.37 ± 0.22	0.11	1.10
5	23.43 ± 5.21	15.27	31.60	1.81 ± 0.55	0.90	4.01
6	25.46 ± 4.04	17.89	31.99	0.92 ± 0.56	0.24	4.85

The climatology obtained for SST for all the clusters in the GC showed a marked seasonality. The mean of cluster 1 (coast of Sinaloa) was 25.99 °C, with a maximum value of 31.98 °C and a minimum value of 16.98 °C (Table 3). The mean SSTs in the central region (clusters 3 and 6) were 24.59 °C and 25.46 °C, and in the southern region (clusters 4 and 2), the means were 26.29 and 26.83 °C. Cluster 5 was the coolest all year.

Figure 5 shows that the annual mean SST increased from the northern to the southern region (R = −0.99), with a coefficient of determination of R^2 = 0.985, and the opposite occurred with the Chl-a concentration; on average, it increased from south to north (R = 0.80), with a coefficient of determination of R^2 = 0.643. The concentration of Chl-a showed the same marked seasonality. Cluster 5 (the northernmost region) presented the highest concentration of Chl-a throughout the year. Cluster 4 (GC western entrance) showed the lowest Chl-a concentrations from throughout the year (Table 3, Figure 4).

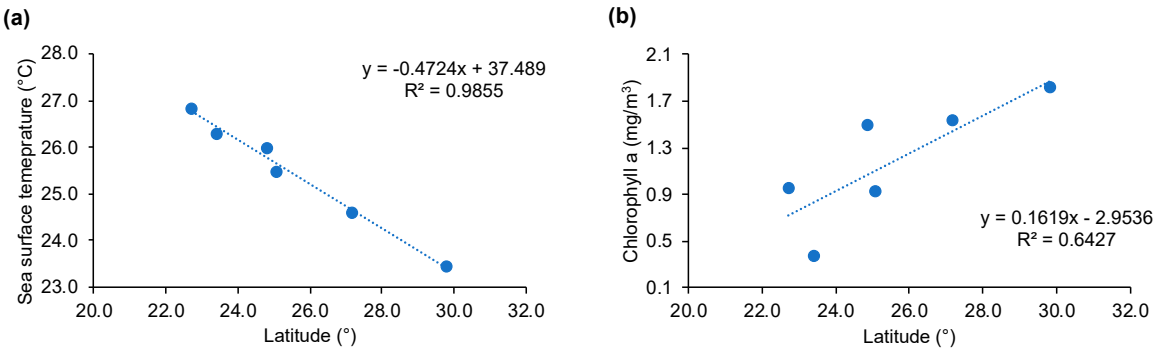

Figure 5. Trends of the annual mean SST (**a**) and Chl-a (**b**) concentration of each cluster in relation to their mean latitude in the GC during the period from 1998–2022.

The mean SST and Chl-a concentration of all clusters showed a high inverse correlation (R = –0.819) with a high coefficient of determination (R^2 = 0.670) (Figure 6). Some variation was exhibited—high values of Chl-a and high SSTs, which was probably because of the vertical and tidal mixing, which are important modes of variation at the sampling stations.

Figure 7 shows the seasonality, annual evolution, and transitional period (scattergram) of the Chl-a concentration and SST in the GC by using the mean fits of the clusters' climatological Chl-a versus SST values. All of the points in the climatological array of the clusters within the GC region were fitted. The distribution of the monthly values in the climatological band indicates that the winter bloom occurs for temperatures lower than 23 °C, when strong north winds alongshore mainland coast are more intense, causing the Ekman transport to increase upwelling events and creating the conditions for the high primary productivity observed along the east coast of the GC [37,38], while the summer non-bloom period (June to September) begins above 27 °C, when high solar radiation causes strong stratification in the mixed layer; although there are upwellings on the west coast of GC generated by weak southern winds, they are of lesser intensity [12]. This

winter bloom differs in timing from the annual blooms of other parts of the GC (such as the Bay of La Paz), where the main bloom occurs in fall to winter, with a secondary bloom in spring [72].

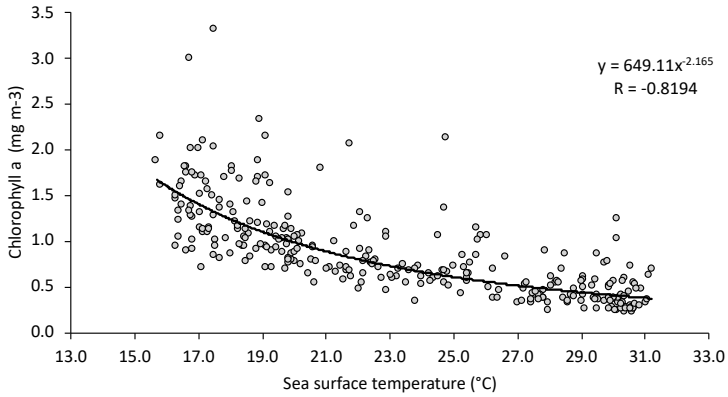

Figure 6. Correlation of SST and Chl-a concentration in the GC during the period from 1998–2022.

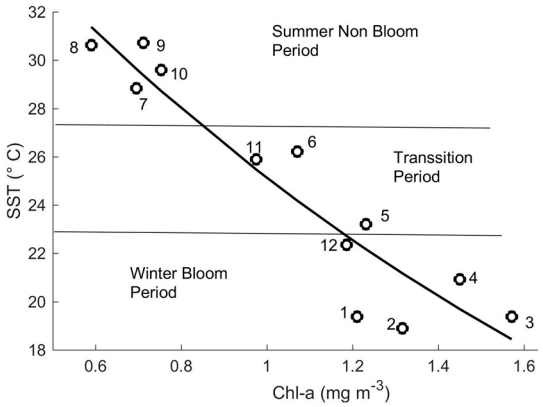

Figure 7. Exponential relationship between the monthly averages Chl-a and SST in the Gulf of California. The numbers in the plot indicate the value for the corresponding month of the year.

3.3. Interannual Variability

Figure 8 shows the annual evolution of the mean SST and Chl-a in the GC during la Niña conditions (such as in 1999), El Niño conditions (2015), and average conditions (2019). Summer conditions start as early as late May during El Niño conditions, whereas during La Niña conditions, they begin during late June. Winter conditions during El Niño are shortened to last from late December to March, while during La Niña conditions, they begin in December and end in May (Figure 8a). As for the Chl-a concentration during El Niño conditions, the winter blooming period is present from January to March, whereas during La Niña conditions, it is from December to May; a higher Chl-a concentration is also noticeable during summer under La Niña conditions in comparison to El Niño and average conditions (Figure 8b).

The interannual variability was predominant with respect to the seasonal variability. Under strong La Niña conditions (1999), relatively warm water (>25 °C) was found near the entrance of the Gulf, while under average conditions (2019), it reached the central region; under strong El Niño conditions (2015), it reached up to the Midriff Islands. To obtain a statistically reliable estimate of the trends of Chl-a and SST for the GC over the last two decades, the monthly time series of the Chl-a and SST anomalies were smoothed twice with a 12-month running mean; the smoothed series and the linear trends are shown in Figure 9. The correlation coefficient, the effective degrees of freedom (*Edf*), and the confidence interval were estimated according to the method Davis [73] and Trenberth [74]. For the Chl-

a anomalies, a decrease of 0.25 ± 0.05 mg/m^3 was obtained, and for the SST anomalies, an increase of 0.73 ± 0.15 °C over 20 years was obtained, as shown in Figure 9. Both correlation coefficients ($R_{Chl\text{-}a}$ = 0.46 and R_{sst} = 0.50) had a weak coefficient of determination (R^2 = 0.21 and R^2 = 0.25, respectively), meaning that the straight lines were moderately significant and explained ~40–45% of the variability of both parameters. The observed trend was probably part of the combined interannual and interdecadal variability of the PO [75], which was unresolved by the short length of the records used here (~25 years).

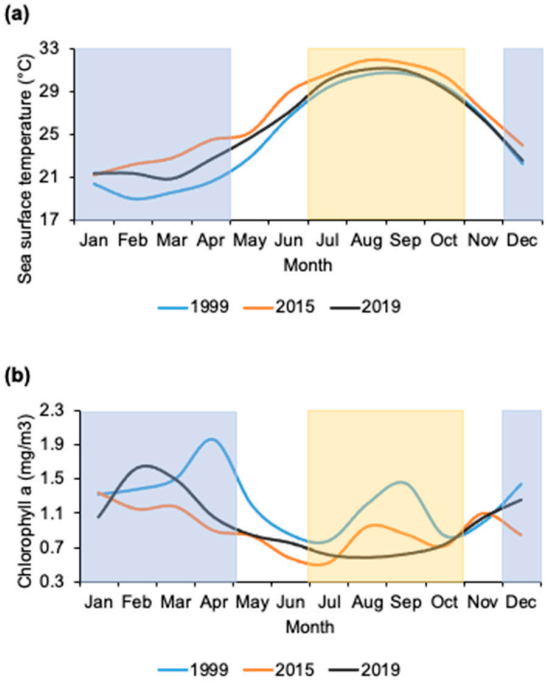

Figure 8. Annual evolution of the mean sea surface temperature (**a**) and chlorophyll *a* (**b**) in the GC under La Niña conditions (1999), El Niño conditions (2015), and average conditions (2019). The blue bar represents the average winter bloom period, and the brown bar represents the average summer non-bloom period in the GC, resultant of Figure 7.

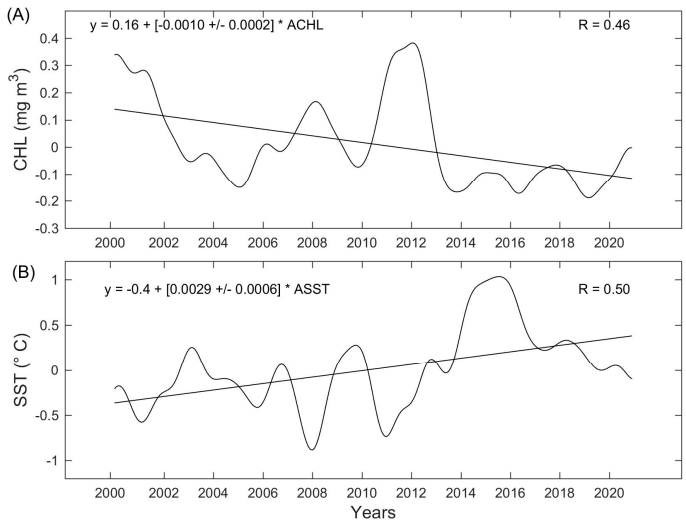

Figure 9. Low-passed series of monthly averages of: (**A**) Chl-a and (**B**) SST anomalies in the GC after the removal of the annual cycle. The 12-month running mean was passed twice. The least-squares linear fit is also shown.

3.4. Fourier Analyses

The spectral analysis of the SST showed that the main frequencies of variation were annual, interannual, and decadal (3 to 7 years and 10–12 years) in most of the clusters (Figure 10). In cluster 5, which is the northernmost region of the GC, a 3-year cycle with a peak power of 12.28 was the most important, followed by a 12-year cycle with a peak power of 11.38, whereas in the clusters from the central GC (clusters 3 and 6), the most important cycles were of 12 years (peak power = 16.36) and 18 years (peak power = 14.30), respectively. On the other hand, the main cycle of the southernmost cluster (2) was of 13 years (peak power = 17.35), followed by a 6-year cycle (peak power = 10.33). In cluster 1, which was the most coastal one, a 16-year cycle was the most important (peak power = 15.83). On the other hand, the spectral analysis of the Chl-a estimated that the main frequency was the interannual one (5 to 10 years), with peak power between 10.60 and 16.08 for most of the clusters with the exception of cluster 5, whose main frequency was of 3 years (peak power = 8.29).

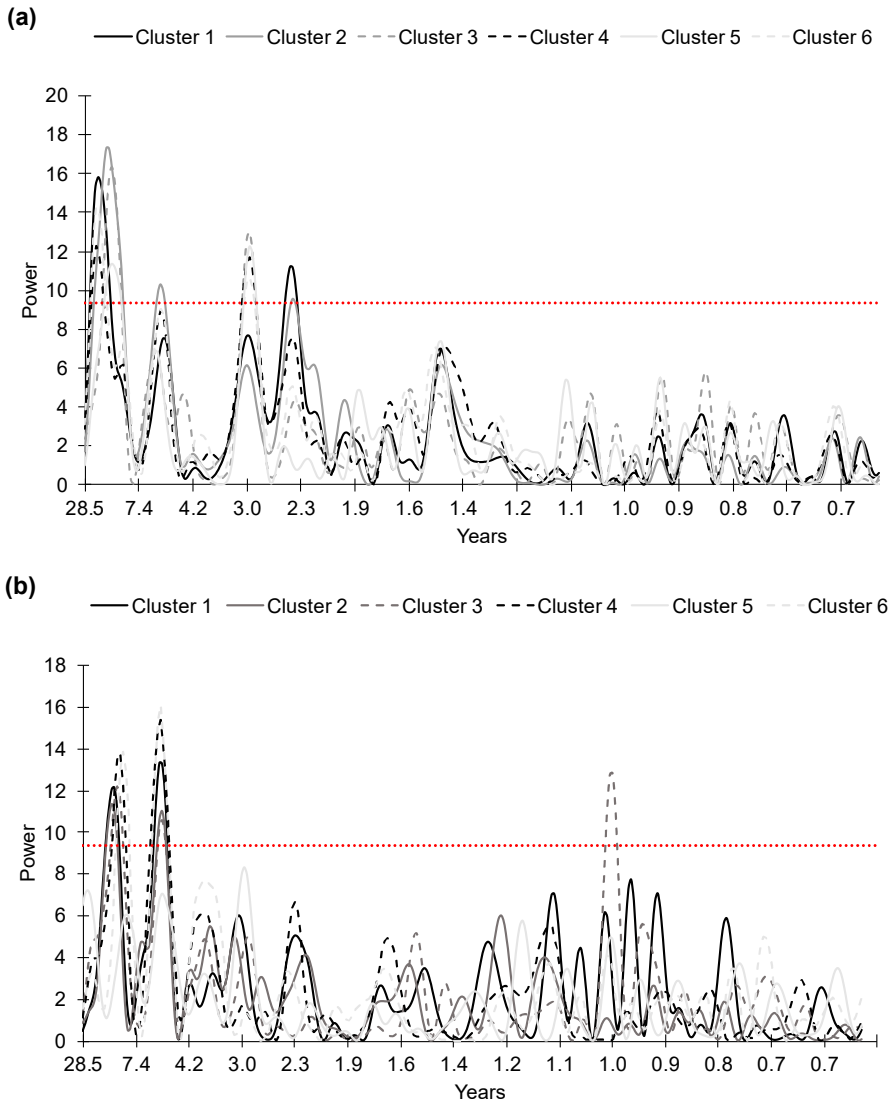

Figure 10. Spectral analysis of the SST (**a**) and Chl-a concentration (**b**) for each cluster in the GC.

3.5. Mesoscale Processes, SST, and Chl-a Concentration

Figure 11 shows the mean SST and Chl-a concentration of 2010–2011 for cluster 5; during summer conditions (Figure 11A,B), long filaments from the Midriff Islands carrying relatively cooler water with high concentration of Chl-a towards the northern GC were

identified. In addition, a cyclonic eddy formed, and it comprised a great area of the northern region. During winter and spring (Figure 11C,D), anticyclonic eddies were identified, mostly in the western side of the northern GC.

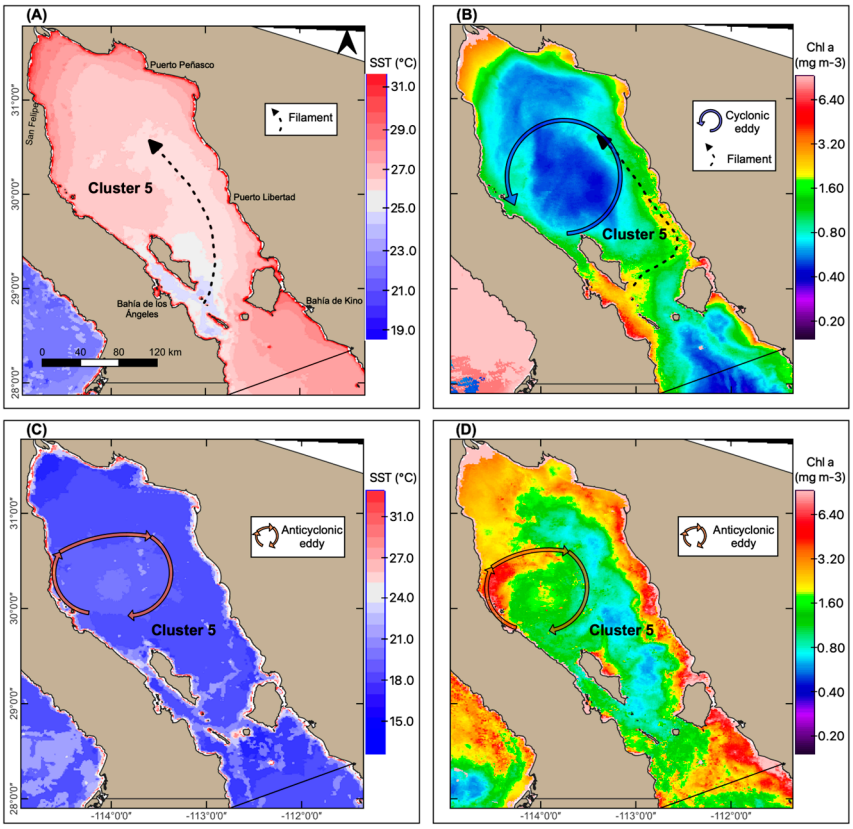

Figure 11. Oceanic mesoscale events identified in the northern GC (cluster 5) during summer (**A**,**B**) and during winter (**C**,**D**) from a composite of the mean conditions of SST and Chl-a satellite images of 2010 and 2011.

In the mean SST and Chl-a concentration of 2010–2011 for clusters 1–4 and 6, the central and southern GC exhibited several eddies with different rotations year-round (Figure 12). In the central region (cluster 3 and northern portion of 6), the outer edges of the eddies reached both coasts of the gulf during most of their lifespans. Moreover, during winter, northwestern winds act parallel to the eastern coast, inciting coastal upwelling in this region, while the southeastern winds during summer act along the western coast, causing a less-intense coastal upwelling; filaments can be seen along both coasts during the coastal upwelling periods. In the southern region (cluster 4), a series of anticyclonic eddies were identified, mostly over the oceanic region. In cluster 1, the effects of northwestern winds over the coast that generate coastal upwelling are seen due to the high Chl-a concentration over this region (Figure 12A,B).

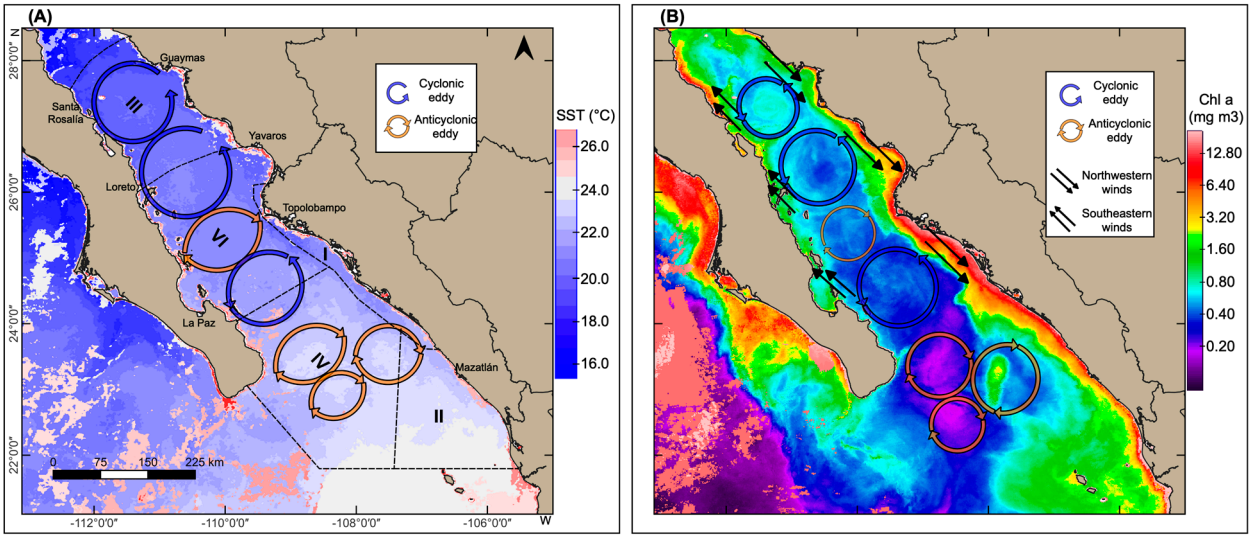

Figure 12. Oceanic mesoscale events identified in the central and southern GC from a composite of the mean conditions of SST (**A**) and Chl-a (**B**) satellite images of 2010 and 2011. Roman numerals indicate the number of the cluster, while discontinuous lines indicate the limits of each cluster.

3.6. Association of the SST and Chl-a Concentration with Climate Indices (ONI and PDO)

According to the cross-correlation of Figure 13a, it takes about 2–4 months for ENSO to reach the GC, inducing increase in the SST, whereas it takes about 4 months for the ENSO to exhibit effects on the Chl-a, decreasing its concentration (Figure 13b). Similarly, an increase in the SST occurs around 3–11 months as associated with PDO, while the Chl-a concentration decreases at around 5–14 months related to PDO (Figure 3d).

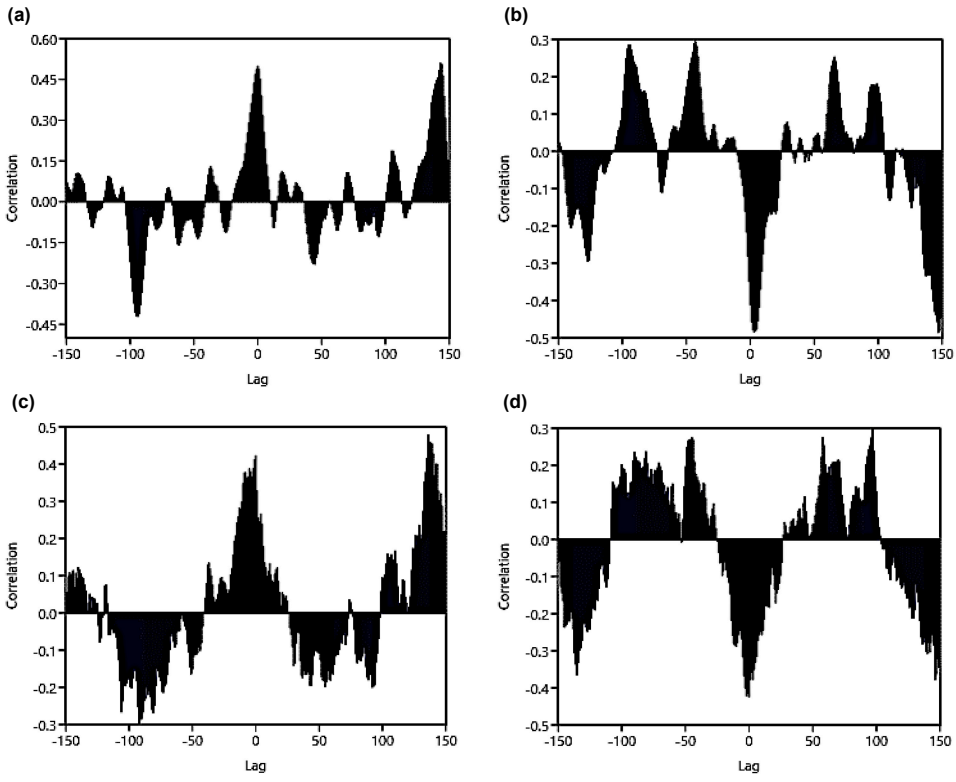

Figure 13. Cross-correlation of the ONI with the mean SST (**a**) and Chl-a concentration (**b**) and the PDO with the mean SST (**c**) and Chl-a concentration (**d**) in the GC during the period from 1998–2022. The Lag is in months.

According to the Spearman rank-correlation, the mean SST and Chl-a concentration showed a significant ($p < 0.05$) correlation (R = 0.440 and R = −0.448, respectively) with the ONI, while with the PDO the correlation was relatively lower for SST (R = 0.379) and for Chl-a (R = −0.445). Regarding the Pearson linear correlation, the coefficients were similar: in for SST and Chl-a, the relationship was (R = 0.498 and R = −0.411, respectively). On the other hand, the relationship with the PDO was (R = 0.422 for SST and R = −0.424 for Chl-a) (Table 4).

Table 4. Rank-correlation (Spearman) and linear correlation (Pearson) analysis ($p < 0.05$) between the ONI index, PDO index, and the time series of SST and Chl-a of the GC for the period from 1998–2021.

Spearman Rank-Correlation ($p < 0.05$)		
	SST	**Chl-a**
ONI	0.440	−0.448
PDO	0.379	−0.445
Pearson Linear Correlation ($p < 0.05$)		
	SST	**Chl-a**
ONI	0.498	−0.411
PDO	0.422	−0.424

4. Discussion

Because the GC is in a transition zone, it exhibits a temperate–tropical climate, while its adjacent continental regions present an arid climate in its northern portion and a subhumid tropical climate in its southeastern portion. These characteristics lead to complex ocean–atmosphere interactions that regulate its environmental variability [3,27,33,76,77]. As it is in a transition zone, the seasonal and interannual modes of variation dominate in the GC [34,40,47], which was confirmed by the results of this study focusing on the oceanography variability of the GC, including its southern portion, which is an area with a significant flow of energy and exchange of properties with the PO [47]. In addition, the seasonal and non-seasonal variability and the connection of the SST and Chl-a during the period from 1998–2022 were analyzed by means of a cluster analysis. The GC is an area that exhibits high biological productivity [1,2,35] and is affected by the presence of remote forcing, which is mainly associated with ENSO signals. The climate variability due to ENSO events in the GC has been studied, but strong controversy remains about the ecological impacts of ENSO [1,5,9,10,76,78]. The biophysical coupling between Chl-a and SST was found (Figures 7 and 8).

The division of marine ecosystems into large regions allows a comprehensive study of their climatological and biological processes, which could have an impact on the distribution and abundance of organisms [53] by producing unique habitats, communities, and ecosystems; it would, thus, be necessary to exploit and manage them independently. Globally, Longhurst et al. [79] proposed the division of the oceans into 57 biogeochemical provinces based on the regional physical oceanography and net primary production. The GC was considered as part of the Central American Coast [53,79,80].

Round [81] proposed the division of the GC into four regions: mouth, south, center, and north. Subsequently, on the basis of the abundance and composition of diatoms, Allen [53] and Cupp and Allen [82] separated it into three areas: (1) the region south of 25°N (southern oceanic), (2) the region between 25° and 27°N (central), and (3) the gulf north of 27°N (northern). Gilbert and Allen [83] differentiated the inner region of the gulf north of 29°N, and they considered the northern gulf as the area between 27° and 29°N. The divisions were preserved by Gilbert and Allen [83], and these divisions corresponded to between the antinodes of Sverdrup [84], who theorized a standing internal wave along the axis of the gulf. Santamaría-del-Ángel et al. [85] divided it into 14 biogeographic regions after analyzing Chl-a satellite images from the 1978–1986 period.

Arias-Aréchiga [50] divided it into three regions considering the primary productivity—north, center, and south—while Soto-Mardones et al. [86] divided the gulf into four regions (north, Midriff Islands, center, and south) based on satellite data on the SST. Lluch-Cota and Arias-Aréchiga [55] divided the northern region proposed by Arias-Aréchiga [50], adding the Ballenas Channel region based on its high Chl-a concentrations. Lavín et al. [46] divided the gulf into four regions based on SST anomalies from the 1984–2000 period.

Recently, different regionalizations have been proposed by several authors [33,51,52,87–89]. Heras-Sánchez et al. [52] suggested the division of the area into 12 regions. The most recent characterization of the regions in the GC by Robles-Tamayo et al. [36] involved the analysis of 24 priority marine regions in the Pacific and GC through monthly Chl-a values.

In this study, the monthly SST and Chl-a data from 513 sampling stations were extracted. Six regions were obtained for both the SST and Chl-a data as a result of the cluster analysis of the 513 sampled stations, and each region was characterized by a distinct SST and Chl-a concentration (Table 2). The differences and strengths of the analysis applied in this study are the following: (1) the higher spatial resolution of the data (1 km), (2) the longer time series of the data (1998–2022), and (3) the consideration of mesoscale processes (eddies and filaments) for the first time, which allowed the potential mechanisms of the concentration and dispersal of Chl-a and temperature to be explained with higher precision. If the locations of eddies and filaments are examined in the area of cluster 5, it can be noted that during summer, long filaments from the Midriff Islands carried relatively cooler water with a higher Chl-a concentration towards the northern GC (Figure 11A,B). Additionally, a cyclonic eddy formed in this region every summer (Figure 11B). However, during winter and spring, anticyclonic eddies were identified (Figure 11c,d). In the central and southern GC (cluster 3 and 6), several eddies with different rotations were identified year-round, where the northern boundary of cluster 3 and southern boundary of cluster 6 seemed to be associated with the edges of the eddies (Figure 12A,B). On the other hand, the high Chl-a concentration from cluster 1 was associated with the wind regime responsible for winter–spring coastal upwelling. At the entrance of the GC (cluster 4), a series of eddies, mostly anticyclonic, were found to contribute in the retention of the high Chl-a concentration in regions far from the coast (Figure 12B).

The variability of the environmental variables analyzed in the six regions is the result of the patterns of atmospheric circulation and seasonal winds [89–91], which established clear differences in the annual SSTs and Chl-a concentrations. These variables also exhibited variations based on a range of latitudinal characters in the zonal component of the gulf, which, together with the influence of mountain ranges on the circulation patterns, resulted in the variability of SST and Chl-a. The regions in the GC were also the result of the atmospheric circulation pattern, which determined the seasonal variability and was characterized by a warm and a cool period, which established an annual cycle with effects on both environmental variables. Even though years with distinct climatic and oceanographic conditions were included in this study, the results agree with what was reported by Heras-Sánchez et al. [52]. The climatology in the GC showed a marked seasonality. The temporal evolution of the pigment concentration presented two regimens throughout the year: the winter–spring bloom period from December to April and the summer non-bloom period from July to October (Figure 7). Transitions occurred in two periods: in spring (May and June), when thermal stratification started, and in autumn (November), when northwestern wind forcing started, and destratification within the gulf occurred, as shown in the study carried out by Robles-Tamayo [39].

The main source of productivity in the GC is due to upwelling events, the most important being those that occur on the east coast of the GC [37,38] and that occur in the cold season, when the northwesterly winds are more intense, causing the Ekman transport to increase, increasing the upwelling of nutrient-rich bottom waters to the surface and thus enriching the water, which in turn increases the phytoplankton biomass and therefore primary production [34,39]. During the warm season of the year, although there are upwellings on the west coast of GC generated by southeasterly winds, they are of lesser

intensity [12]. All the above explains the inverse relationship between SST and Chl a. Other events winds of a different nature occur in the region of the Ballenas-Salsipuedes Channel, and upwellings occur throughout the year and are generated by mixing and turbulence processes due to changes in bathymetry [92].

This average weather pattern is substantially modified during El Niño and La Niña events since the cold season of the year does not occur during El Niño; even in that period, the warmest months occur, coinciding with what happens in the countries from South America, Ecuador and Peru (referring to its name, El Niño) [93]. During La Niña events, the opposite occurs; that is, the warm season is absent throughout the year.

Contrary to what was previously described as occurring regarding Chl-a, during average years, the months with the highest Chl-a concentration occur from January to May and a second smaller maximum from October to December; that is, the highest Chl-a concentration values occur in the cold season of the year, conforming to the relationship shown in the Figure 6. This pattern is also modified during warm and cold events, increasing productivity in the GC during cold events. This can be explained by the fact that in La Niña years, the northwesterly winds intensify and upwelling increases due to the Ekman effect [34].

The annual mean SST increased, and the Chl-a decreased from north to south in the gulf. Soto-Mardones [86] and Heras-Sánchez et al. [52] reported similar results. At the southern limit and mouth of the gulf, warm waters from the PO predominated [94,95] and had effects on the average conditions that reached the Agiabampo–Loreto Bay area (26°N). However, during La Niña, these effects were evident north of the state of Sinaloa and south of Bahía La Paz (24°N). Under El Niño conditions, the water from the Pacific reached the region of 29°N (Ángel de La Guarda Island and Tiburon Island, Figure 11). Additionally, in the Fourier series analysis, the cycles associated with ENSO events were obvious in all of the clusters (Table 4, Figure 10).

In the GC, the transition to the warm period occurs during June, resulting in an increase in the SST due to the advection process as a result of the direct interaction with the PO. This allows tropical subsurface water, which is warmer than the GC water [90,96], to enter the gulf. This causes a significant stratification process, which inhibits the effects of coastal upwelling along the western coast from July to October (summer–autumn), together with relatively weaker southeasterly winds [82]. However, the transition to the cold period starts during November and lasts from December to May (winter–spring), resulting in strong northwesterly seasonal winds that incite coastal upwelling and mixing processes along the eastern coast of the GC, thus increasing the phytoplanktonic biomass [34,85,86,97]. Moreover, other mechanisms such as tide mixing and direct interaction with the PO, which determine oceanographic conditions in the GC, favor high levels of phytoplanktonic material, which increases the Chl-a concentration.

The SST has an important variability in the gulf due to the dynamics of the water column, particularly through the effects of tidal mixing, upwelling events, and seasonal wind patterns, especially in the region of the Midriff Islands [98] and in the northern GC [89]. This effect was reported by López et al. [99] and Álvarez-Molina et al. [100] in the Ballenas Channel, where the SST decreased due to the constant flux of currents and tidal mixing, which generated very particular circulation in the area in comparison with other areas of the gulf. Upwelling of deep water with high content of nutrients, which enhanced the high Chl-a concentrations and primary productivity, was regularly produced. These characteristics make the region an important area of biomass concentration of commercially important species such as small pelagic fish, which are food for many other commercially and ecologically important species.

As shown in the graph of the climatology (Figure 4) and the scattergram of SST and Chl-a in Figure 7, the values support the seasonal progression. The values of Chl-a and SST fell within the climatological band in the GC with Chl-a (between +1.0 and 1.5 mg/m^3). The distribution indicated that bloom occurred for temperatures lower than 23.2 °C (winter), while the non-bloom period began above 27.5 °C (summer). May, June, and November

fell outside these SST criteria (transition period) (Figure 7). In the spectral analysis of the clusters in the SST and Chl-a, predominant cycles of 3–7 years were estimated and were associated with ENSO events (10 a,b) with a mean lag of 4 months (Figure 13), and cycles of 10–20 years were found to be related to the PDO (Figure 10, Table 4) in all of the regions.

The combination of SST and Chl-a data in carrying out the clustering analysis allowed us to obtain the bioregions with the greatest statistical certainty; the clusters are bioregions that represent types of habitats (sets of local physical, chemical, and biological characteristics) that provide an environment for biota since a habitat is the integration of the characteristics of seawater that determine the potential for biological communities [101,102]. This is crucial because the quantity and quality of available habitats largely determine the structure and composition of communities [102,103]. Three of the regions found in this study coincide with the fish communities obtained by Acevedo-Cervantes et al. [104] in deep areas and by Rábago-Quiroz et al. [105] in areas near the coast of the GC. Acevedo-Cervantes [106] postulated that the biogeographical overlap of the fauna in the GC is a reflection of (1) the gulf's geographic position (at the limits of the distribution of species with affinities for temperate, tropical, and temperate–warm transition environments), (2) the regions that characterize the GC (north, center, and south), and (3) oceanographic events that develop in the gulf, which generate a vigorous circulation that interacts with the variable depth to create a spectrum of kinetic energy with well-defined periods. These produce events of high dynamism that support marine fauna and flora and benefit fish by allowing them to establish themselves and dwell in areas of high biological productivity [107].

The trend analysis showed that the SST increased while Chl-a decreased during the period of this study. The GC showed a heating trend at an annual rate of 0.03 °C (0.73 °C in 20 years) and a decrease in its productivity at an annual rate of 0.008–0.012 mg/m^3. Although the presence of the cold anomaly related to La Niña in 1999–2000 in combination with the large warm anomaly during ENSO in 2015–2016 helped in the trends observed in Figure 9, there was a non-El-Niño interdecadal signal of Chl-a and SST in the GC that showed decreases (increases) of about ~0.25 mg/m^3 and ~0.7 °C, respectively. McPhaden and Zhang [108] and Lavin et al. [46] (with records of SST anomalies that were previous to the period studied here) showed increases of ~0.8 °C and ~1 °C in the SST in the equatorial Pacific and GC regions, respectively. Herrera-Cervantes et al. [48] showed the trend of the interannual variability of Chl-a, and Robles-Tamayo et al. [39,40] showed that high peaks of the interannual frequencies of SST and Chl-a observed in the southern GC region were associated with global climatological–oceanographic phenomena (ENSO events). Therefore, the trends observed for Chl-a and SST could mainly be driven by interdecadal changes in the equatorial PO.

This agrees with Hakspiel-Segura et al. [95] and Sánchez-Cabeza et al. [48], although it differs in terms of the rate of temperature increase since they estimated a rate of 0.57 ± 0.01 °C per decade, while the rate estimated in our study was ~0.27–0.35 °C. It should be clarified that the region analyzed by Sánchez-Cabeza et al. [48] comprised the shallow coastal waters at the entrance of the GC, which is an area that is under the constant influence of the warmer tropical surface water carried by the Mexican coastal current and under the influence of the PO. This was revealed in the mean annual temperature estimated for this region (cluster 6), which was 27.16 ± 2.96 °C, and its climatology was greater than that of any other region in the GC.

On the other hand, Hakspiel-Segura et al. [97] concluded that the Pacific Meridional Mode (PMM) is the principal mode of variation in the GC. The PMM modulates the development of the ENSO [109]. Since the PMM can be driven by the North Pacific Oscillation [110–112], tropical North Atlantic SST anomalies [113], and the anomalous Kuroshio Extension [114], changes in these variabilities potentially strengthen the PMM [115–117]. The authors concluded that because global warming favors the growth of the PMM, it will exert a greater impact on ENSO [109].

These conditions (warming and reduction of productivity) in the GC will have repercussions at the ecosystem level by modifying its communities and ecosystems. For example, Gilly et al. [118] stated that this trend has likely changed trophic webs throughout the GC and impacted many taxa, including small pelagic fish (as they are forage fish), as well as larger teleost fishes; the authors concluded that a long-term pattern of decline is emerging across multiple taxa [118]. Coastal ecosystems are especially vulnerable to climatic variability and the impacts of climate change. Increasing the SST induces changes of species dwelling relevant ecosystems [2,47,119,120], affects primary production [121], and generates changes in populations of marine organisms [47,122]. All of the variabilities shown here induce variable conditions that generate different habitats and could explain the high biodiversity of the GC.

This environmental change that is taking place alters the biophysical and ecological properties of the ocean, affecting life at various levels of functional organization, such as genes, species, populations, and communities, and modifying the routes of food chains and even generating distribution of species [123], favoring some and affecting others. We believe that more than a decline in the ecosystems, there may be a replacement of species of the communities that inhabit the Gulf of California (dissociation of communities), predominating species of tropical affinity and decreasing species of temperate affinity and the increase of invasive species, in addition to favoring the population growth of some species such as coelenterates (which are structuring ecosystems due to their voracity), for example, the jellyfish, which in recent years has been the object of fisheries worldwide. This change can affect food security, necessitating public policies aimed at achieving the adaptation of socio-ecological systems.

5. Conclusions

In this work, by using the monthly averages of composite satellite images of SST (°C) and Chl-a (mg/m^3), we showed with a descriptive analysis of the SST and Chl-a series that the SST and the amplitude of the warm period decreased from south to north (the cold period increased from south to north). By means of a cluster analysis of the SST and Chl-a concentration, six bioregions were identified. The six bioregions showed that the main frequencies in the SST were annual and interannual, and the frequencies of variation were associated with basin-level weather events such as El Niño and La Niña. In addition, cycles of 10–13 and 15–20 years were identified. The cycle of 10–13 years explained almost 40–50% of the signal power in some regions. The SST and Chl-a showed a heating trend at an annual rate of ~0.036 °C (~0.73 °C over 20 years) and a decrease in productivity at an annual rate of ~0.012 mg/m^3 (~0.25 mg/m^3 over 20 years). Moreover, mesoscale features (eddies and filaments) were identified in the GC, and they were mainly associated with the clusters of the SST and Chl-a. All of the variability shown here induced variable conditions that generated different habitats and could explain the high biodiversity of the GC. If the warming trend in the SST and the decreasing trend in the Chl-a continue in the long term, this could raise concern, as they can have important effects on the dynamics of this important ecosystem, which could be less resilient to future environmental disturbances, including habitat loss for numerous native species, thus supporting the arrival of harmful invasive species.

Author Contributions: Conceptualization, J.L.M., H.H.C. and R.G.M.; data curation, E.B.F.E. and R.G.M.; formal analysis, J.L.M., E.B.F.E. and H.H.C.; funding acquisition, J.L.M.; investigation, J.L.M., E.B.F.E., H.H.C. and R.G.M.; methodology, J.L.M., E.B.F.E., H.H.C. and R.G.M.; project administration, J.L.M.; resources, J.L.M.; software, J.L.M., E.B.F.E., H.H.C. and R.G.M.; supervision, J.L.M. and H.H.C.; validation, J.L.M., E.B.F.E., H.H.C. and R.G.M.; visualization, J.L.M., E.B.F.E. and H.H.C.; writing—original draft, J.L.M., E.B.F.E. and H.H.C.; writing—review and editing, J.L.M., E.B.F.E. and H.H.C. All authors have read and agreed to the published version of the manuscript.

Funding: This research was funded by the project CONAHCYT Pronace 2017-2018-01-A3-S-77965.

Acknowledgments: We acknowledge Eloisa Herrera and Rufino Morales of the Fisheries Laboratory of CIBNOR Guaymas.

Conflicts of Interest: The authors declare no conflict of interest.

References

1. Lluch-Cota, S.E.; Aragón-Noriega, E.A.; Arreguín-Sánchez, F.; Aurioles-Gambóa, D.; Bautista-Romero, J.J.; Brusca, R.C.; Cervantes-Duarte, R.; Cortés-Altamirano, R.; Del-Monte-Luna, P.; Esquivel-Herrera, A.; et al. The Gulf of California: Review of ecosystem status and sustainability challenges. *Prog. Oceanogr.* **2007**, *73*, 1–26. [CrossRef]
2. Páez-Osuna, F.; Sanchez-Cabeza, J.A.; Ruiz-Fernández, A.C.; Alonso-Rodríguez, R.; Piñón-Gimate, A.; Cardoso-Mohedano, J.G.; Flores-Verdugo, F.J.; Carballo, J.L.; Cisneros-Mata, M.A.; Álvarez-Borrego, S. Environmental status of the Gulf of California: A review of responses to climate change and climate variability. *Earth-Sci. Rev.* **2016**, *162*, 253–268. [CrossRef]
3. Duque-Herrera, A.F.; Helenes, J.; Flores-Trujillo, J.G.; Ruiz-Fernández, A.C.; Sánchez-Cabeza, J.A. Dinoflagellate cysts and ENSO-PDO climate forcing in the southern Gulf of California. *Palaeogeogr. Palaeoclimatol. Palaeoecol.* **2020**, *560*, 110055. [CrossRef]
4. Castro, R.; Durazo, R.; Mascarenhas, A.; Collins, C.A.; Trasviña, A. Thermohaline variability and geostrophic circulation in the southern portion of the Gulf of California. *Deep-Sea Res. Pt. I.* **2006**, *53*, 188–200. [CrossRef]
5. López-Martínez, J.; Arreguín-Sánchez, F.; Hernández-Vázquez, S.; García-Juárez, A.R.; Valenzuela-Quiñonez, W. Interannual variation of growth of the brown shrimp *Farfantepenaeus californiensis* and its relation to temperature. *Fish. Res.* **2003**, *61*, 95–105. [CrossRef]
6. López-Martínez, J.; Rábago-Quiroz, C.; Nevárez-Martínez, M.O.; García-Juárez, A.R.; Rivera-Parra, G.; Chávez-Villalba, J. Growth, reproduction, and size at first maturity of blue shrimp, *Litopenaeus stylirostris* (Stimpson, 1874) along the east coast of the Gulf of California, Mexico. *Fish. Res.* **2005**, *71*, 93–102. [CrossRef]
7. López-Martínez, J. *La Variabilidad Ambiental y las Pesquerías de México*; Comisión Nacional de Acuacultura y Pesca: México D.F., México, 2008; pp. 1–200.
8. Lanz, E.; López-Martínez, J.; Nevárez-Martínez, M.; Dworak, J.A. Small pelagic fish catches in the Gulf of California associated with sea surface temperature and chlorophyll. *Calif. Coop. Ocean. Fish. Investig. Rep.* **2009**, *50*, 134–146.
9. Giron-Nava, A.; Ezcurra, E.; Brias, A.; Velarde, E.; Deyle, E.; Cisneros-Montemayor, A.M.; Munch, S.B.; Sugihara, G.; Aburto-Oropeza, O. Environmental variability and fishing effects on the Pacific sardine fisheries in the Gulf of California. *Can. J. Fish. Aquat. Sci.* **2021**, *78*, 623–630. [CrossRef]
10. Farach-Espinoza, E.B.; López-Martínez, J.; García-Morales, R.; Nevarez-Martínez, M.O.; Ortega-García, S.; Lluch-Cota, D.B. Coupling oceanic mesoscale events with catches of the Pacific sardine (*Sardinops sagax*) in the Gulf of California. *Prog. Oceanogr.* **2022**, *206*, 102858. [CrossRef]
11. Castro, R.; Lavín, M.F.; Ripa, P. Seasonal heat balance in the Gulf of California. *J. Geophys. Res-Ocean.* **1994**, *99*, 3249–3261. [CrossRef]
12. Lluch-Cota, S.E. Coastal upwelling in the eastern Gulf of California. *Oceanol. Acta.* **2000**, *23*, 731–740. [CrossRef]
13. Figueroa, J.M.; Robles, J.M. Eddies in the Gulf of California. In Proceedings of the Oceanography Society Inaugural Meeting, Monterey, CA, USA, 27–30 August 1989.
14. Oschlies, A.; Garçon, V. Eddy-induced enhancement of primary production in a model of the North Atlantic. *Nature* **1998**, *394*, 266–269. [CrossRef]
15. López-Calderón, J.; Manzo-Monroy, H.; Santamaría-del-Ángel, E.; Castro, R.; González-Silvera, A.; Millán-Núñez, R. Mesoscale variability of the Mexican Tropical Pacific using TOPEX and SeaWiFS data. *Cienc. Mar.* **2006**, *32*, 539–549. [CrossRef]
16. Fu, L.-L.; Chelton, D.B.; Le Traon, P.-Y.; Morrow, R. Eddy Dynamics From Satellite Altimetry. *Oceanography* **2010**, *23*, 14–25. [CrossRef]
17. Alpers, W.; Brandt, P.; Lazar, A.; Dagorne, D.; Sow, B.; Faye, S.; Hansen, M.W.; Rubino, A.; Poulain, P.-M.; Brehmer, P. A small-scale oceanic eddy off the coast of West Africa studied by multi-sensor satellite and surface drifter data. *Remote Sens. Environ.* **2013**, *129*, 132–143. [CrossRef]
18. Cruz Gómez, R.C.; Monreal Gómez, M.A.; Nikolaevich Bulgakov, S. Efecto de los vórtices en sistemas acuáticos y su relación con la química, biología y geología. *Interciencia* **2008**, *33*, 741–746.
19. Kahru, M.; Fiedler, P.C.; Gille, S.T.; Manzano, M.; Mitchell, B.G. Sea level anomalies control phytoplankton biomass in the Costa Rica Dome area. *Geophys. Res. Lett.* **2007**, *34*, 1–5. [CrossRef]
20. Kahru, M.; Mitchell, B.G.; Gille, S.T.; Hewes, C.D.; Holm-Hansen, O. Eddies enhance biological production in the Weddell-Scotia Confluence of the Southern Ocean. *Geophys. Res. Lett.* **2007**, *34*, 1–6. [CrossRef]
21. Dufois, F.; Hardman-Mountford, N.J.; Greenwood, J.; Richardson, A.J.; Feng, M.; Matear, R.J. Anticyclonic eddies are more productive than cyclonic eddies in subtropical gyres because of winter mixing. *Sci. Adv.* **2016**, *2*, e1600282. [CrossRef]
22. Gaube, P.; Chelton, D.B.; Samelson, R.M.; Schlax, M.G.; O'Neill, L.W. Satellite Observations of Mesoscale Eddy-Induced Ekman Pumping. *J. Phys. Oceanogr.* **2015**, *45*, 104–132. [CrossRef]
23. Wang, Y.; Zhang, H.-R.; Chai, F.; Yuan, Y. Impact of mesoscale eddies on chlorophyll variability off the coast of Chile. *PLoS ONE* **2018**, *13*, e0203598. [CrossRef] [PubMed]

24. Chaigneau, A.; Eldin, G.; Dewitte, B. Eddy activity in the four major upwelling systems from satellite altimetry (1992–2007). *Prog. Oceanogr.* **2009**, *83*, 117–123. [CrossRef]
25. Nan, F.; Xue, H.; Xiu, P.; Chai, F.; Shi, M.; Guo, P. Oceanic eddy formation and propagation southwest of Taiwan. *J. Geophys. Res. Ocean.* **2011**, *116*, 1–15. [CrossRef]
26. Ripa, P. Seasonal circulation in the Gulf of California. *Ann. Geophys.* **1990**, *8*, 559–563.
27. Ripa, P. Toward a Physical Explanation of the Seasonal Dynamics and Thermodynamics of the Gulf of California. *J. Phys. Oceanogr.* **1997**, *27*, 597–614. [CrossRef]
28. Beier, E.; Ripa, P. Seasonal gyres in the northern Gulf of California. *J. Phys. Oceanogr.* **1999**, *29*, 305–311. [CrossRef]
29. Palacios-Hernández, E.; Beier, E.; Lavín, M.F.; Ripa, P. The effect of the seasonal variation of stratification on the circulation of the northern Gulf of California. *J. Phys. Oceanogr.* **2002**, *32*, 705–728. [CrossRef]
30. Beron-Vera, F.J.; Ripa, P. Three-dimensional aspects of the seasonal heat balance in the Gulf of California. *J. Geophys Res–Ocean.* **2000**, *105*, 11441–11457. [CrossRef]
31. Beron-Vera, F.J.; Ripa, P. Seasonal salinity balance in the Gulf of California. *J. Geophys Res.–Ocean.* **2002**, *107*, 15-1–15-15. [CrossRef]
32. Castro, R.; Mascarenhas, A.S.; Durazo, R.; Collins, C.A. Seasonal variation of the temperature and salinity at the entrance to the Gulf of California, Mexico. *Cienc. Mar.* **2000**, *26*, 561–583. [CrossRef]
33. Lavin, M.F.; Marinone, S.G. An Overview of the Physical Oceanography of the Gulf of California. In *Nonlinear Processes in Geophysical Fluid Dynamics*; Velasco Fuentes, O.U., Sheinbaum, J., Ochoa, J., Eds.; Kluwer Academic Publishers: Dordrecht, The Netherlands, 2003; pp. 173–204.
34. García-Morales, R.; López-Martínez, J.; Valdez-Holguin, J.E.; Herrera-Cervantes, H.; Espinosa-Chaurand, L.D. Environmental Variability and Oceanographic Dynamics of the Central and Southern Coastal Zone of Sonora in the Gulf of California. *Remote Sens.* **2017**, *9*, 925. [CrossRef]
35. Farach-Espinoza, E.B.; López-Martínez, J.; García-Morales, R.; Nevárez-Martínez, M.O.; Lluch-Cota, D.B.; Ortega-García, S. Temporal variability of oceanic mesoscale events in the Gulf of California. *Remote Sens.* **2021**, *13*, 1774. [CrossRef]
36. Robles-Tamayo, C.M.; García-Morales, R.; Romo-León, J.R.; Figueroa-Preciado, G.; Peñalba-Garmendia, M.C.; Enríquez-Ocaña, L.F. Variability of Chl-a Concentration of Priority Marine Regions of the Northwest of Mexico. *Remote Sens.* **2022**, *14*, 4891. [CrossRef]
37. Badan-Dangon, A.; Dorman, C.E.; Merrifield, M.A.; Winant, C.D. The lower atmosphere over the Gulf of California. *J. Geophys. Res. Ocean.* **1991**, *96*, 16877–16896. [CrossRef]
38. Turrent, C.; Zaitsev, O. Seasonal cycle of the near-surface diurnal wind field over the bay of La Paz, Mexico. *Bound-Lay Meteorol.* **2014**, *151*, 353–371. [CrossRef]
39. Robles-Tamayo, C.M.; García-Morales, R.; Valdez-Holguín, J.E.; Figueroa-Preciado, G.; Herrera-Cervantes, H.; López-Martínez, J.; Enríquez-Ocaña, L.F. Chlorophyll a concentration distribution on the mainland coast of the Gulf of California, Mexico. *Remote Sens.* **2020**, *12*, 1335. [CrossRef]
40. Robles-Tamayo, C.M.; Valdez-Holguín, J.E.; García-Morales, R.; Figueroa-Preciado, G.; Herrera-Cervantes, H.; López-Martínez, J.; Enríquez-Ocaña, L.F. Sea Surface Temperature (SST) Variability of the Eastern Coastal Zone of the Gulf of California. *Remote Sens.* **2018**, *10*, 1434. [CrossRef]
41. Lluch-Cota, S.E.; Parés-Sierra, A.; Magaña-Rueda, V.O.; Arreguín-Sánchez, F.; Bazzino, G.; Herrera-Cervantes, H.; Lluch-Belda, D. Changing climate in the Gulf of California. *Prog. Oceanogr.* **2010**, *87*, 114–126. [CrossRef]
42. Strub, P.T.; James, C. Altimeter-derived surface circulation in the large–scale NE Pacific Gyres.: Part 1. seasonal variability. *Prog. Oceanogr.* **2002**, *53*, 163–183. [CrossRef]
43. Latif, M.; Barnett, T.P. Causes of decadal climate variability over the North Pacific and North America. *Science.* **1994**, *266*, 634–637. [CrossRef]
44. Filonov, A.; Tereshchenko, I. El Niño 1997–98 monitoring in mixed layer at the Pacific Ocean near Mexico's west coast. *Geophys. Res. Lett.* **2000**, *27*, 705–707. [CrossRef]
45. Herrera-Cervantes, H.; Lluch-Cota, D.B.; Lluch-Cota, S.E.; Gutiérrez-de-Velasco, S. The ENSO signature in sea-surface temperature in the Gulf of California. *J. Mar. Res.* **2007**, *65*, 589–605. [CrossRef]
46. Lavín, M.F.; Palacios-Hernández, E.; Cabrera, C. Sea surface temperature anomalies in the Gulf of California. *Geofís. Int.* **2003**, *42*, 363–375. [CrossRef]
47. Sánchez-Cabeza, J.A.; Herrera-Becerril, C.A.; Carballo, J.L.; Yáñez, B.; Álvarez-Sánchez, L.F.; Cardoso-Mohedano, J.G.; Ruiz-Fernández, A.C. Rapid surface water warming and impact of the recent (2013–2016) temperature anomaly in shallow coastal waters at the eastern entrance of the Gulf of California. *Prog. Oceanogr.* **2022**, *202*, 102746. [CrossRef]
48. Herrera-Cervantes, H.; Lluch-Cota, S.E.; Lluch-Cota, D.B.; Gutiérrez de Velasco Sanromán, G.; Lluch-Belda, D. ENSO influence on satellite-derived chlorophyll trends in the Gulf of California. *Atmósfera* **2010**, *23*, 253–262.
49. Belda, D.L.; del Monte Luna, P.; Lluch-Cota, S.E. 20th century variability in Gulf of California SST. *Cal. Coop. Ocean. Fish.* **2009**, *50*, 147–154.
50. Arias-Aréchiga, J.P. Regionalización del Golfo de California: Una Propuesta a Partir de Concentración de Pigmentos Fotosintéticos. Bachelor Thesis, Universidad Autónoma de Baja California Sur, La Paz, Bolivia, 1998.
51. Petatán-Ramírez, D. Propuesta de Zonación del Golfo de California con Base en Variables Oceanográficas y Distribución de Macroinvertebrados. Master thesis, Universidad Autónoma de Baja California Sur, La Paz, Bolivia, 2015.

52. Heras-Sánchez, M.d.C.; Valdez-Holguín, J.E.; Hazas-Izquierdo, R.G. Sea-Surface Temperature Spatiotemporal Analysis for the Gulf of California, 1998–2015: Regime Change Simulation. In *Supercomputing. ISUM 2018. Communications in Computer and Information Science*; Torres, M., Klapp, J., Gitler, I., Tchernykh, A., Eds.; Springer: Cham, Switzerland, 2019; Volume 948, pp. 167–181.
53. Allen, W.E. Plankton diatoms of the Gulf of California obtained by the G. Allan Hancock Expedition of 1936. *Allan Hancock Pac. Exped.* **1937**, *3*, 47–59.
54. Flores-de-Santiago, F.J.; Santamaría-del-Ángel, E.; González-Silvera, A.; Martínez-Díaz-de-León, A.; Millán-Núñez, R.; Kovacs, J.M. Assessing dynamics micro-regions in the Great Islands of the Gulf of California based on MODIS aqua imagery products. In Proceedings of the Coastal Ocean Remote Sensing, San Diego, CA, USA, 5 October 2007.
55. Lluch-Cota, S.E.; Arias-Aréchiga, J.P. Sobre la importancia de considerar la existencia de centros de actividad biológica para la regionalización del océano: El caso del Golfo de California. In *Centros de Actividad Biológica del Pacífico Mexicano*; Lluch-Belda, D., Elourduy-Garay, J.F., Lluch-Cota, S.E., Ponce-Díaz, G., Eds.; Centro de Investigaciones Biológicas del Noroeste, SC: La Paz, Mexico, 2000; pp. 255–263. ISBN 970-18-6285-6.
56. Jiménez, A.; Marinone, S.G.; Parés-Sierra, A. Efecto de la variabilidad espacial y temporal del viento sobre la circulación en el Golfo de California. *Ciencias Mar.* **2005**, *31*, 357–368. [CrossRef]
57. Lavín, M.F.; Castro, R.; Beier, E.; Godínez, V.M.; Amador, A.; Guest, P. SST, thermohaline structure, and circulation in the southern Gulf of California in June 2004 during the North American Monsoon Experiment. *J. Geophys. Res. Ocean.* **2009**, *114*, 1–22. [CrossRef]
58. Kahru, M. Windows Image Manager, WIM Software (Ver. 9.06) and User's Manual. 2016, p. 125. Available online: http://www.wimsoft.com/ (accessed on 28 June 2017).
59. Bitácora Ambiental Golfo de California. Available online: https://www.gob.mx/semarnat/acciones-y-programas/bitacora-ambiental-golfo-de-california (accessed on 23 July 2023).
60. Ralambondrainy, H. A conceptual version of the k-means algorithm. *Pattern Recognit. Lett.* **1995**, *16*, 1147–1157. [CrossRef]
61. Koren, O.; Hallin, C.A.; Perel, N.; Bendet, D. Decision-making enhancement in a big data environment: Application of the k-means algorithm to mixed data. *J. Artif. Intell. Soft Comput. Res.* **2019**, *9*, 293–302. [CrossRef]
62. Li, L.; Wang, J.; Li, X. Efficiency analysis of machine learning intelligent investment based on K-means algorithm. *IEEE Access.* **2020**, *8*, 147463–147470. [CrossRef]
63. MacQueen, J. Some methods for classification and analysis of multivariate observations. In Proceedings of the Fifth Berkeley Symposium on Mathematical Statistics and Probability, Los Angeles, CA, USA, 21 June–18 July 1965; Cambridge University Press: London, UK, 1967; Volume 1, pp. 281–297.
64. Mantua, N.J.; Hare, S.R.; Zhang, Y.; Wallace, J.M.; Francis, R.C. A Pacific interdecadal climate oscillation with impacts on salmon production. *B. Am. Meteorol. Soc.* **1997**, *78*, 1069–1080. [CrossRef]
65. Pegau, W.S.; Boss, E.; Martínez, A. Ocean color observations of eddies during the summer in the Gulf of California. *Geophys. Res. Lett.* **2002**, *29*, 6-1–6-3. [CrossRef]
66. Cayula, J.-F.; Cornillon, P. Edge Detection Algorithm for SST Images. *J. Atmos. Ocean. Technol.* **1992**, *9*, 67–80. [CrossRef]
67. Diehl, S.F.; Budd, J.W.; Ullman, D.; Cayula, J.-F. Geographic Window Sizes Applied to Remote Sensing Sea Surface Temperature Front Detection. *J. Atmos. Ocean. Technol.* **2002**, *19*, 1105–1113. [CrossRef]
68. Marinone, S.G.; Ulloa, M.J.; Parés-Sierra, A.; Lavín, M.F.; Cudney-Bueno, R. Connectivity in the northern Gulf of California from particle tracking in a three-dimensional numerical model. *J. Mar. Syst.* **2008**, *71*, 149–158. [CrossRef]
69. Álvarez-Borrego, S. *Physical Oceanography in a New Island Biogeography of the Sea of Cortes*; Case, T.J., Cody, M.L., Ezcurra, E., Eds.; Oxford University Press: New York, NY, USA, 2002; pp. 41–59.
70. López, M.; Candela, J.; García, J. Two overflows in the Northern Gulf of California. *J. Geophys. Res.-Ocean.* **2008**, *113*, 1–12. [CrossRef]
71. Lavín, M.F.; Castro, R.; Beier, E.; Godínez, V.M. Mesoscale eddies in the southern Gulf of California during summer: Characteristics and interaction with the wind stress. *J. Geophys. Res.-Ocean.* **2013**, *118*, 1367–1381. [CrossRef]
72. Herrera-Cervantes, H. Sea surface temperature, ocean color and wind forcing patterns in the Bay of La Paz, Gulf of California: Seasonal variability. *Atmósfera* **2019**, *32*, 25–38. [CrossRef]
73. Davis, R.E. Predictability of sea surface temperature and sea level pressure anomalies over the North Pacific Ocean. *J. Phys. Oceanog.* **1976**, *6*, 249–266. [CrossRef]
74. Trenberth, K.E. What are the seasons? *Bull. Am. Meteorol.* **1983**, *64*, 1276–1282. [CrossRef]
75. Miller, A.J.; Schneider, N. Interdecadal climate regime dynamics in the North Pacific Ocean: Theories, observations and ecosystem impacts. *Prog. Oceanogr.* **2000**, *47*, 355–379. [CrossRef]
76. Lavín, M.F.; Durazo, R.; Palacios, E.; Argote, M.L.; Carrillo, L. Lagrangian Observations of the Circulation in the Northern Gulf of California. *J. Phys. Oceanogr.* **1997**, *27*, 2298–2305. [CrossRef]
77. Lanz-Sánchez, E.E. Análisis de la Variabilidad Espacio-Temporal en la Disponibilidad de las Especies de Pelágicos Menores en el Golfo de California y su Relación con el Medio Ambiente. Doctoral Thesis, Centro de Investigaciones Biológicas del Noroeste, La Paz, Bolivia, 2008.

78. Hernández-Padilla, J.C.; Zetina-Rejón, M.J.; Arreguín-Sánchez, F.; del Monte-Luna, P.; Nieto-Navarro, J.T.; Salcido-Guevara, L.A. Structure and function of the southeastern Gulf of California ecosystem during low and high sea surface temperature variability. *Reg. Stud. Mar. Sci.* **2021**, *43*, 101686. [CrossRef]
79. Longhurst, A.; Sathyendranath, S.; Platt, T.; Caverhill, C. An estimate of global primary production in the ocean from satellite radiometer data. *J. Plankton Res.* **1995**, *17*, 1245–1271. [CrossRef]
80. Reygondeau, G.; Longhurst, A.; Martinez, E.; Beaugrand, G.; Antoine, D.; Maury, O. Dynamic biogeochemical provinces in the global ocean. *Global Biogeochem. Cycles.* **2013**, *27*, 1046–1058. [CrossRef]
81. Round, F.E. The phytoplankton of the Gulf of California. Part I. Its composition, distribution and contribution to the sediments. *J. Exp. Mar. Biol. Ecol.* **1967**, *1*, 76–97. [CrossRef]
82. Cupp, E.E.; Allen, W.A. Plankton diatoms of the Gulf of California. *Allan Hancock Pac. Exped.* **1938**, *3*, 61–99.
83. Gilbert, J.Y.; Allen, W.E. The phytoplankton of the Gulf of California obtained by the E.W. Scripps in 1939 and 1940. *J. Mar. Res.* **1943**, *5*, 89–110.
84. Sverdrup, H.U. The Gulf of California: Preliminary discussion of the cruise of the E.W. Scripps in February and March 1939. *Pac. Sci. Cong.* **1941**, *3*, 161–166.
85. Santamaría-del-Angel, E.; Alvarez-Borrego, S.; Müller-Karger, F.E. Gulf of California biogeographic regions based on coastal zone color scanner imagery. *J. Geophys. Res. Ocean.* **1994**, *99*, 7411–7421. [CrossRef]
86. Soto-Mardones, L.; Marinone, S.G.; Parés-Sierra, A. Time and spatial variability of sea surface temperature in the Gulf of California. *Cienc. Mar.* **1999**, *25*, 1–30. [CrossRef]
87. Kahru, M.; Marinone, S.G.; Lluch-Cota, S.E.; Parés-Sierra, A.; Mitchell, B.G. Ocean-color variability in the Gulf of California: Scales from days to ENSO. *Deep Sea Res. 2 Top Stud. Oceanogr.* **2004**, *51*, 139–146. [CrossRef]
88. Lluch-Cota, D. El sector pesquero. In *Cambio Climático: Una Visión Desde México*; Martínez, J., Fernández, A., Eds.; Secretaria de Medio Ambiente y Recursos Naturales, Instituto Nacional de Ecología: México D.F., México, 2004; pp. 327–335.
89. Escalante, F.; Valdez-Holguín, J.E.; Álvarez-Borrego, S.; Lara-Lara, J.R. Temporal and spatial variation of sea surface temperature, chlorophyll a, and primary productivity in the Gulf of California. *Cienc. Mar.* **2013**, *39*, 203–215. [CrossRef]
90. Álvarez-Borrego, S. Gulf of California. In *Estuaries and Enclosed Seas*; Ketchum, B.H., Ed.; Elsevier: New York, NY, USA, 1983; pp. 427–449.
91. Álvarez-Borrego, S.; Lara-Lara, J.R. The Physical environment and primary productivity of the Gulf of California. In *The Gulf and Peninsular Province of the Californias*; Dauphin, J.P., Simoneit, B.R.T., Eds.; AAPG Mem: Tulsa, OK, USA, 1991; pp. 555–567.
92. Martínez-Díaz-de-León, A.; Pacheco-Ruíz, I.; Delgadillo-Hinojosa, F.; Zertuche-González, J.A.; Chee-Barragán, A.; Blanco-Betancourt, R.; Guzmán-Calderón, J.M.; Gálvez-Telles, A. Spatial and temporal variability of the sea surface temperature in the Ballenas-Salsipuedes Channel (central Gulf of California). *J. Geophys. Res.-Ocean.* **2006**, *111*, 1–7. [CrossRef]
93. Solomon, S.; Qin, D.; Manning, M.; Chen, Z.; Marquis, M.; Averyt, K.B.; Tignor, M.; Miller, H.L. (Eds.) Climate Change 2007: The Physical Science Basis. Contribution of Working Group I to the Fourth Assessment Report of the Intergovernmental Panel on Climate Change. Cambridge University Press: Cambridge, UK, 2007; pp. 235–336.
94. Gutiérrez, O.Q.; Marinone, S.G.; Parés-Sierra, A. Lagrangian surface circulation in the Gulf of California from a 3D numerical model. *Deep. Sea Res. Part II Top. Stud. Oceanogr.* **2004**, *51*, 659–672. [CrossRef]
95. Lavín, M.F.; Castro, R.; Beier, E.; Cabrera, C.; Godínez, V.M.; Amador-Buenrostro, A. Surface circulation in the Gulf of California in summer from surface drifters and satellite images (2004–2006). *J. Geophys. Res. Ocean.* **2014**, *119*, 4278–4290. [CrossRef]
96. Torres-Orozco, E. Volumetric Analysis of the Water Masses of the Gulf of California. MSc. Thesis, Centro de Investigación Científica y de Educación Superior de Ensenada, Ensenada, México, 1993.
97. Hakspiel-Segura, C.; Martínez-López, A.; Delgado-Contreras, J.A.; Robinson, C.J.; Gómez-Gutiérrez, J. Temporal variability of satellite chlorophyll-a as an ecological resilience indicator in the central region of the Gulf of California. *Prog. Oceanogr.* **2022**, *205*, 102825. [CrossRef]
98. Robles, J.M.; Marinone, S.G. Seasonal and interannual thermohaline variability in the Guaymas Basin of the Gulf of California. *Cont. Shelf Res.* **1987**, *7*, 715–733. [CrossRef]
99. López, M.; Candela, J.; Argote, M.L. Why does the Ballenas Channel have the coldest SST in the Gulf of California? *Geophys. Res. Lett.* **2006**, *33*, 1–5. [CrossRef]
100. Álvarez-Molina, L.L.; Álvarez-Borrego, S.; Lara-Lara, J.R.; Marinone, S.G. Annual and semiannual variations of phytoplankton biomass and production in the central Gulf of California estimated from satellite data. *Cienc. Mar.* **2013**, *39*, 217–230. [CrossRef]
101. Aadland, L.P. Stream habitat types: Their fish assemblages and relationship to flow. *N. Am. J. Fish. Manag.* **1993**, *13*, 790–806. [CrossRef]
102. Gómez, N.; Cochero, J. Un índice para evaluar la calidad del hábitat en la Franja Costera Sur del Río de la Plata y su vinculación con otros indicadores ambientales. *Ecol. Austral.* **2013**, *23*, 18–26. [CrossRef]
103. Borja, A.; Bald, J.; Franco, J.; Larreta, J.; Muxika, I.; Revilla, M.; Germán Rodríguez, J.; Solaun, O.; Uriarte, A.; Valencia, V. Using multiple ecosystem components, in assessing ecological status in Spanish (Basque Country) Atlantic marine waters. *Mar. Pollut. Bull.* **2009**, *59*, 54–64. [CrossRef] [PubMed]
104. Acevedo-Cervantes, A.; López-Martínez, J.; Herrera-Valdivia, E.; Rodríguez-Romero, J. Análisis de la abundancia, dominancia y diversidad de la comunidad de peces demersales de profundidad de 90 a540 metros en el Golfo de California, México. *Interciencia* **2009**, *34*, 660–665.

105. Rábago-Quiroz, C.H.; López-Martínez, J.; Valdez-Holguín, J.E.; Nevárez-Martínez, M.O.; Acevedo-Cervantes, A. Fish assemblages in the bycatch of bottom shrimp trawls on the west side of the Gulf of California, Mexico. *Mar. Biol. Res.* **2012**, *8*, 865–876. [CrossRef]
106. Acevedo-Cervantes, A. Composición Espacial y Temporal de los Peces Acompañantes del Camarón de Profundidad del Golfo de California. Ph.D. Thesis, Universidad Autónoma de Nayarit, Nayarit, México, 2010.
107. Rodríguez-Romero, J.; del Carmen López-González, L.; Galván-Magaña, F.; Sánchez-Gutiérrez, F.J.; Inohuye-Rivera, R.B.; Pérez-Urbiola, J.C. Seasonal changes in a fish assemblage associated with mangroves in a coastal lagoon of Baja California Sur, Mexico. *Lat. Am. J. Aquat. Res.* **2011**, *39*, 250–260. [CrossRef]
108. McPhaden, M.J.; Zhang, D. Slowdown of the meridional overturning circulation in the upper Pacific Ocean. *Nature* **2002**, *415*, 603–608. [CrossRef]
109. Fan, H.; Yang, S.; Wang, C.; Wu, Y.; Zhang, G. Strengthening amplitude and impact of the Pacific meridional mode on ENSO in the warming climate depicted by CMIP6 models. *J. Clim.* **2022**, *35*, 5195–5213. [CrossRef]
110. Walker, G.T.; Bliss, E.W. World Weather V. *Mem. Roy. Met. Soc.* **1932**, *4*, 53–84. [CrossRef]
111. Rogers, J.C. The north Pacific oscillation. *Int. J. Climatol.* **1981**, *1*, 39–57. [CrossRef]
112. Linkin, M.E.; Nigam, S. The North Pacific Oscillation–west Pacific teleconnection pattern: Mature-phase structure and winter impacts. *J. Clim.* **2008**, *21*, 1979–1997. [CrossRef]
113. Ham, Y.G.; Kug, J.S.; Park, J.Y.; Jin, F.F. Sea surface temperature in the north tropical Atlantic as a trigger for El Niño/Southern Oscillation events. *Nat. Geosci.* **2013**, *6*, 112–116. [CrossRef]
114. Joh, Y.; Di Lorenzo, E. Interactions between Kuroshio Extension and Central Tropical Pacific lead to preferred decadal-timescale oscillations in Pacific climate. *Sci. Rep.* **2019**, *9*, 13558. [CrossRef] [PubMed]
115. Park, J.H.; Li, T.; Yeh, S.W.; Kim, H. Effect of recent Atlantic warming in strengthening Atlantic–Pacific teleconnection on interannual timescale via enhanced connection with the Pacific meridional mode. *Clim. Dyn.* **2019**, *53*, 371–387. [CrossRef]
116. Chen, B.; Xie, L.; Zheng, Q.; Zhou, L.; Wang, L.; Feng, B.; Yu, Z. Seasonal variability of mesoscale eddies in the Banda Sea inferred from altimeter data. *Acta Oceanol. Sin.* **2020**, *39*, 11–20. [CrossRef]
117. Chen, C.; He, X.; Lu, Y.; Chu, Y. Application of Landsat time-series data in island ecological environment monitoring: A case study of Zhoushan Islands, China. *J. Coast. Res.* **2020**, *108*, 193–199. [CrossRef]
118. Gilly, W.; Markaida, U.; Daniel, P.; Frawley, T.; Robinson, C.; Gómez-Gutiérrez, J.; Hyun, D.; Soliman, J.; Pandey, P.; Rosenzweig, L. Long-term hydrographic changes in the Gulf of California and ecological impacts: A crack in the World's Aquarium? *Prog. Oceanogr.* **2022**, *206*, 102857. [CrossRef]
119. Wong, S.N.; Whitehead, H. Seasonal occurrence of sperm whales (*Physeter macrocephalus*) around Kelvin Seamount in the Sargasso Sea in relation to oceanographic processes. *Deep-Sea Res. I Oceanogr. Res. Pap* **2014**, *91*, 10–16. [CrossRef]
120. Pörtner, H.O.; Karl, D.M.; Boyd, P.W.; Cheung, W.; Lluch-Cota, S.E.; Nojiri, Y.; Schmidt, D.N.; Zavialov, P.O.; Alheit, J.; Aristegui, J.; et al. Ocean Systems. In *Climate Change 2014: Impacts, Adaptation, and Vulnerability. Part A: Global and Sectoral Aspects. Contribution of Working Group II to the Fifth Assessment Report of the Intergovernmental Panel on Climate Change*; Field, C., Barros, V., Dokken, D., Mach, K., Mastrandrea, M., Bilir, T., Chatterjee, M., Ebi, K., Estrada, Y., Genova, R., et al., Eds.; Cambridge University Press: Cambridge, UK; New York, NY, USA, 2014; pp. 411–484.
121. Behrenfeld, M.J.; Boss, E. Beam attenuation and chlorophyll concentration as alternative optical indices of phytoplankton biomass. *J. Mar. Res.* **2006**, *64*, 431–451. [CrossRef]
122. Pinsky, M.L.; Worm, B.; Fogarty, M.J.; Sarmiento, J.L.; Levin, S.A. Marine taxa track local climate velocities. *Science* **2013**, *341*, 1239–1242. [CrossRef]
123. Coll, M.; Bellido, J.M.; Pennino, M.G. Cómo Proteger las Sardinas y Anchoas Mediterráneas de la Sobrepesca y el Cambio Climático. Available online: https://digital.csic.es/handle/10261/261558 (accessed on 28 July 2023).